Induced Orbital Paramagnetism and Paratropism in Closed-Shell Molecules†

Stefano Pelloni and Paolo Lazzeretti*

Dipartimento di Chimica dell'Università degli Studi di Modena, Via Campi 183, 41100 Modena, Italy

Riccardo Zanasi

Dipartimento di Chimica dell'Università degli Studi di Salerno, Via Ponte don Melillo, 84084 Fisciano (SA), Italy

Received: April 27, 2009; Revised Manuscript Received: June 8, 2009

Three-dimensional models of the quantum-mechanical current density induced by a uniform magnetic field in the electron cloud have been obtained for closed-shell systems BeH^-, BH, and CH^+, characterized by induced orbital paramagnetism, and in planar unsaturated hydrocarbons C_4H_4 and clamped C_8H_8, exhibiting π paramagnetism. It is shown that, even for these paramagnetic systems, the paramagnetic contributions to magnetic susceptibilities and nuclear magnetic shielding, customarily taken into account in perturbation theory approaches, can formally be eliminated via the procedure of continuous transformation of the origin of the current density−paramagnetic zero. The definition of magnetic response properties can therefore be recast as a sum of two formally "diamagnetic" terms for any molecule, including systems showing strong induced orbital paramagnetism. It is shown that the paramagnetism in the compounds studied arises from the nodal topology of the electronic wave function. In particular, paratropic vortices circulate about stagnation lines at the intersection of nodal surfaces of the highest-occupied zero-order molecular orbital and corresponding first-order orbital.

1. Introduction

Diamagnetism is defined as a property "characteristic of materials that line up at right angles to a nonuniform magnetic field and that partly expel from their interior the magnetic field in which they are placed".[1] Such a behavior was first observed (1778) by S. J. Brugmans of Leyden University in bismuth and by Le Baillif (1827) in antimony; see p 144 of *Light and Electricity* by John Tyndall.[2] However, the term "diamagnetism" was coined by Michael Faraday, who started studying it systematically in 1845 and discovered that all substances in nature exhibit some form of diamagnetic response to an applied magnetic field.

Diamagnetism is independent of temperature, and it is typical of elements and compounds that possess complete sets of valence electrons, referred to as shells, in which all their electrons are paired. Since two paired electrons have opposite spins, the magnetic field generated by each spinning electron is canceled out by the magnetic field of the other. When such a species with closed electron shells is placed in a magnetic field, it is repelled. However, the response of some substances to the magnetic perturbation is just the opposite, that is, paramagnetic.

Paramagnetism is characteristic of materials attracted by a strong magnet. It generally occurs in elements or compounds possessing unpaired, singly orbiting electrons, whose motion generates a magnetic field. Such substances behave as a permanent magnet, for example, if placed in a magnetic field, their intrinsic field aligns with, and hence strengthen, the applied magnetic field. Paramagnetism decreases with rising temperature because alignment is partially lost due to the greater random motion of the elementary magnets. However, temperature-independent weak paramagnetism is observed in many metallic elements in the solid state, such as sodium and the other alkali metals.

Quite remarkably, temperature-independent paramagnetism has also been predicted for closed-shell diatomic molecules with six valence electrons, boron monohydride BH,[3−18] the CH^+ cation,[15,17,18] and the BeH^- anion.[17,18] Paramagnetic contributions to the out-of-plane component of the magnetic susceptibility tensor arise from ring currents sustained by the π electrons in monocyclic conjugated hydrocarbons, for instance, cyclobutadiene C_4H_4,[19,20] and in flattened cyclo-octatetraene (COT) C_8H_8 annelated with perfluorocyclobuteno moieties[21] and with bicyclo[2.1.1] hex-2-ene groups.[22,23] π-Electron paramagnetism is also exhibited by polycyclic systems.[24,25] Remarkable examples are corannulene and coronene dianions.[26]

According to the van Leeuwen's theorem quoted in Section 24, p 94, of the book by van Vleck,[27] the magnetic susceptibilities and the induced magnetic moments vanish when classical Boltzmann statistics are applied to any dynamical system.[28] Therefore, in the words of Feynman, "*it is not possible* to understand the magnetic effects of materials in any honest way from the point of view of classical physics. Magnetic response is a *completely quantum mechanical phenomenon*".[29] Possibly, the need for a quantum mechanical approach is even stronger to understand paramagnetism in closed-shell molecules. It can only be explained by a careful analysis of the topology of the electronic wavefunction, which determines the presence of paramagnetic vortices about nodal lines.[6,30−36] Such a behavior has been referred to as *induced orbital paramagnetism*[37] by Riess.[6]

The main purpose of the present investigation is to add further evidence on the source of temperature-independent paramagnetism in diatomics, BH, CH^+, and BeH^-, and of the paratropic ring currents induced in the π electrons of C_4H_4 and clamped

† Part of the "Vincenzo Aquilanti Festschrift".

* Corresponding author.

10.1021/jp903859k
Published on Web 07/13/2009

C_8H_8, by analyzing the topology of magnetic-field induced current density vector field.

The conventional quantum mechanical partition of magnetic quantities into "d" and "p" contributions, currently referred to as "diamagnetic" and "paramagnetic" within the framework of perturbative approaches, for example, for the current density $\mathbf{J}^{\mathbf{B}} = \mathbf{J}^{\mathbf{B}}_{\mathrm{d}} + \mathbf{J}^{\mathbf{B}}_{\mathrm{p}}$, for the magnetizability, $\xi_{\alpha\beta} = \xi^{\mathrm{d}}_{\alpha\beta} + \xi^{\mathrm{p}}_{\alpha\beta}$ (using the symbol recommended by IUPAC), and for the magnetic shielding, $\sigma^{I}_{\alpha\beta} = \sigma^{I\mathrm{d}}_{\alpha\beta} + \sigma^{I\mathrm{p}}_{\alpha\beta}$ at nucleus I, is discussed in Section 2.

Flygare[38] has shown that molecular g factors and magnetizability in molecules can be combined to obtain a direct measurement of the ground-state electronic average of the $\sum_{i=1}^{n} r_i^2$ operator, where r_i is referenced to the center of mass (CM). The molecular g factor is a sum of terms, one depending on the nuclear position, and a second depending on all the excited electronic states of the molecule. The magnetizability is also a sum of term, the first term (diamagnetic susceptibility) depending on the ground electronic state and the second term (paramagnetic susceptibility) depending on all the excited electronic states of the molecule. The excited electronic-state dependence on the molecular g factor and the diamagnetic susceptibility is the same. Thus, if one knows the molecular g factors, the molecular structure, and the average susceptibility, a term depending on the ground electronic molecular state may be obtained, that is, the average $\langle \Psi_a^{(0)} | \sum_{i=1}^{n} r_i^2 | \Psi_a^{(0)} \rangle$. The rotational magnetic moment and the spin-rotational constants of a molecule are related respectively to the paramagnetic term of the susceptibility (gauge origin at CM) and to the paramagnetic term of the nuclear shieldings (gauge origin on the nucleus in question).[38]

However, we emphasize that, in general, the distinction between diamagnetic and paramagnetic parts of magnetic tensors is loose and sometimes misleading, since only the sum of these d and p contributions has a physical meaning. Moreover, the "paramagnetic" part of the current density $\mathbf{J}^{\mathbf{B}}$ may have any direction. It can be either diatropic, that is, flowing clockwise on planes at right angles to the direction of the applied field $\mathbf{B}$, or paratropic, that is, anticlockwise.[39] Current density vector components parallel or antiparallel to $\mathbf{B}$ exist, and they should be taken into account to fulfill the continuity condition $\nabla \cdot \mathbf{J}^{\mathbf{B}} = 0$; however, they do not contribute to the diagonal components of magnetic response tensors.

The erroneous inequality $\xi^{\mathrm{p}}_{\alpha\alpha} < |\xi^{\mathrm{d}}_{\alpha\alpha}|$ presented by Guy, Tillieu, and Baudet (GTB)[40] and the Rebane's method[41,42] based on a gauge transformation that formally kills the paramagnetic $\xi^{\mathrm{p}}_{\alpha\alpha}$ contribution to $\xi_{\alpha\alpha}$ are reviewed in Section 3. Rebane shows that the GTB inequality[40] fails if the electronic wave function for the reference state possesses nodal surfaces. However, he claims that the diamagnetic character of the total magnetizability (that is, the inequality $\xi_{\alpha\alpha} \leqslant 0$) is proven for the ground state,[41] which was shown to be incorrect for closed-shell systems with more than two electrons.[5]

On the other hand, as discussed in Section 4, the "paramagnetic" p contribution to $\mathbf{J}^{\mathbf{B}}$ perpendicular to $\mathbf{B}$ can effectively be killed for molecules with more than two electrons via the procedure of continuous transformation of the origin of the current density−paramagnetic zero (CTOCD-PZ). The "p" parts of the magnetizability $\xi_{\alpha\beta}$ and of the magnetic shielding $\sigma^{I}_{\alpha\beta}$ are also killed.[43−45] Furthermore, it is also demonstrated that the annihilated "paramagnetic" contribution to the current density is merely transformed into a formally "diamagnetic" (non-Larmor) term in disguise. Therefore, the $\mathbf{J}^{\mathbf{B}}(\mathbf{r})$ vector does not change at any point $\mathbf{r}$, as the total current density is invariant to the CTOCD-PZ transformation. Total $\xi_{\alpha\beta}$ and $\sigma^{I}_{\alpha\beta}$ are also invariant; in particular, they stay the same for typically paramagnetic species like BH and CH^+, after formally annihilating $\xi^{\mathrm{p}}_{\alpha\beta}$ and $\sigma^{I\mathrm{p}}_{\alpha\beta}$. In Section 4 the CTOCD-PZ procedure is compared with methods based on a gauge transformation which, like Rebane's, kill the "paramagnetic" contribution to $\xi_{\alpha\alpha}$,[5,41,42] providing a simple counter-argument against the erroneous inequality $\xi^{\mathrm{p}}_{\alpha\alpha} < |\xi^{\mathrm{d}}_{\alpha\alpha}|$.[40]

Models of current density field constructed via the procedures discussed in Section 5 are described in Section 6. An explanation of paramagnetism in closed-shell molecules is provided in Section 7 allowing for topological methods.[6,30−36]

2. Diamagnetic and Paramagnetic Contributions to Magnetic Properties

Within current quantum mechanical theories of magnetic response, the induced electronic current density,[46] the magnetizability,[27] and nuclear magnetic shieldings[47] are expressed as a sum of two parts, referred to as diamagnetic and paramagnetic contributions, respectively. These terms are not uniquely defined; they convert into one another in a gauge transformation of the vector potential (e.g., in a gauge translation, which is equivalent to a change of coordinate system), only their sum being invariant.

Let us consider a closed-shell molecule with n electrons with position $\mathbf{r}_i$, canonical momentum $\hat{\mathbf{p}}_i$, and angular momentum $\hat{\mathbf{l}}_i = \mathbf{r}_i \times \hat{\mathbf{p}}_i$, $i = 1, 2, ..., n$, in a spatially uniform magnetic field $\mathbf{B} = \nabla \times \mathbf{A}$, with vector potential $\mathbf{A} = (1/2)\mathbf{B} \times \mathbf{r}$ in the Coulomb gauge. SI units are used throughout this paper. The zero-order Hamiltonian is $\hat{H}^{(0)} = \hat{T} + \hat{V}$, with $\hat{T} = -\hbar^2/2m_e \sum_{i=1}^{n} \nabla_i^2$. $\hat{V}$ contains electron−nucleus and electron−electron interactions. The unperturbed electronic reference state is described by the real wave function $\Psi_a^{(0)}(\mathbf{x}_1, \mathbf{x}_2, ..., \mathbf{x}_n)$, with $\mathbf{x}_i = \mathbf{r}_i \otimes \eta_i$ a space-spin coordinate and $(\hat{H}^{(0)} - E_a^{(0)})\Psi_a^{(0)} = 0$.

To first-order in $\mathbf{B}$, the quantum mechanical electronic current density can be written as a sum of paramagnetic and diamagnetic contributions,

$$\mathbf{J}^{\mathbf{B}} = \mathbf{J}^{\mathbf{B}}_{\mathrm{p}} + \mathbf{J}^{\mathbf{B}}_{\mathrm{d}} \tag{1}$$

where

$$\mathbf{J}^{\mathbf{B}}_{\mathrm{d}}(\mathbf{r}) = -\frac{e^2}{2m_e}\mathbf{B} \times \mathbf{r}\gamma^{(0)}(\mathbf{r}) \tag{2}$$

is related to the probability density $\gamma^{(0)}$ of the unperturbed molecule. The paramagnetic contribution is given by

$$\mathbf{J}^{\mathbf{B}}_{\mathrm{p}}(\mathbf{r}) = -\frac{ne}{m_e}\int \mathrm{d}\mathbf{x}_2 ... \mathrm{d}\mathbf{x}_n \times [\mathbf{B}\cdot\boldsymbol{\Psi}^{\mathbf{B}}_a{}^{*}(\mathbf{r}, \mathbf{x}_2, ..., \mathbf{x}_n)\hat{\mathbf{p}}\Psi_a^{(0)}(\mathbf{r}, \mathbf{x}_2, ..., \mathbf{x}_n) + \Psi_a^{(0)*}(\mathbf{r}, \mathbf{x}_2, ..., \mathbf{x}_n)\hat{\mathbf{p}}\mathbf{B}\cdot\boldsymbol{\Psi}^{\mathbf{B}}_a(\mathbf{r}, \mathbf{x}_2, ..., \mathbf{x}_n)] \tag{3}$$

introducing the first-order perturbed wave function, an axial vector with components

$$\left|\Psi^{B_\alpha}_a\right\rangle = \frac{1}{\hbar}\sum_{j\neq a}\omega_{ja}^{-1}\left|\Psi_j^{(0)}\right\rangle\left\langle\Psi_j^{(0)}\right|\hat{m}_\alpha\left|\Psi_a^{(0)}\right\rangle \tag{4}$$

where $\hat{m}_\alpha = -(e/2m_e)\sum_{i=1}^{n}\hat{l}_{i\alpha}$ is the magnetic dipole moment of electrons.

The definitions of molecular magnetic properties can be given in concise form allowing for eqs 1−3. Employing tensor notation, and the Einstein implicit summation rule over repeated Greek suffixes, using the Levi-Civita third-rank unit pseudotensor $\varepsilon_{\alpha\beta\gamma}$ and introducing the current density tensor, that is, the derivative[48]

$$\mathscr{T}_{\alpha}^{B_\beta}(\mathbf{r}) = \frac{\partial J_{\alpha}^{\mathbf{B}}(\mathbf{r})}{\partial B_\beta} \tag{5}$$

the magnetizability and the magnetic shielding at nucleus I, with position coordinate $\mathbf{R}_I$, are expressed as integrals in three-dimensional space[49]

$$\xi_{\alpha\delta} = \frac{1}{2}\varepsilon_{\alpha\beta\gamma}\int r_\beta \mathscr{T}_{\gamma}^{B_\delta}(\mathbf{r})\, \mathrm{d}^3 r \tag{6}$$

$$\sigma_{\alpha\delta}(\mathbf{R}_I) \equiv \sigma_{\alpha\delta}^{I} = -\frac{\mu_0}{4\pi}\varepsilon_{\alpha\beta\gamma}\int \frac{r_\beta - R_{I\beta}}{|\mathbf{r} - \mathbf{R}_I|^3}\mathscr{T}_{\gamma}^{B_\delta}(\mathbf{r})\, \mathrm{d}^3 r \tag{7}$$

Whereas the diatropic rotation of the magnetically induced Larmor-type current density (eq 2) is always in such a direction to produce a diamagnetic contribution to the susceptibility—the Langevin-Pauli term[27]

$$\xi_{\alpha\beta}^{\mathrm{d}} = -\frac{e^2}{4m_e}\langle\Psi_a^{(0)}\left|\sum_{i=1}^{n}(r_\gamma{}^2\delta_{\alpha\beta} - r_\alpha r_\beta)_i\right|\Psi_a^{(0)}\rangle \tag{8}$$

the "paramagnetic" contribution to the current density (eq 3) may have any direction. The paramagnetic contribution to the magnetizability in the van Vleck theory[27] is

$$\xi_{\alpha\beta}^{\mathrm{p}} = \frac{1}{\hbar}\sum_{j\neq a}\frac{2}{\omega_{ja}}\mathscr{R}(\langle\Psi_a^{(0)}\left|\hat{m}_\alpha\right|\Psi_j^{(0)}\rangle\langle\Psi_j^{(0)}\hat{m}_\beta\left|\Psi_a^{(0)}\right\rangle) \tag{9}$$

GTB presented a variational approach to calculate magnetic susceptibilities $\xi_{\alpha\beta}$,[50−53] whereby the sum-over-state formula 9 for $\xi_{\alpha\beta}^{\mathrm{p}}$ is replaced by an expectation value over the reference state, much easier to evaluate. Analogous variational schemes have later been described and extended to predict nuclear magnetic shieldings.[54−59] In ref 40, GTB reported a proof that the paramagnetic contribution $\xi_{\alpha\alpha}^{\mathrm{p}}$ cannot be larger than the diamagnetic contribution $|\xi_{\alpha\alpha}^{\mathrm{d}}|$. Their method is related to that developed later by Rebane[41] reviewed in Section 3, as shown by Hegstrom and Lipscomb.[5]

3. Rebane's Approach

Within Rebane's approach, the first- and second-order Hamiltonians are written $\hat{H}^{(1)} = (e/2m_e)\sum_{i=1}^{n}(\mathbf{A}\cdot\hat{\mathbf{p}} + \hat{\mathbf{p}}\cdot\mathbf{A})_i$ and $\hat{H}^{(2)} = (e^2/2m_e^2)\sum_{i=1}^{n}A_i{}^2$, respectively, in an arbitrary gauge for the vector potential. Since the expectation value $\langle\Psi_a^{(0)}|\hat{H}^{(1)}|\Psi_a^{(0)}\rangle$ vanishes, the first-order equation of the Rayleigh−Schrödinger perturbation theory becomes

$$[\hat{H}^{(0)} - E_a^{(0)}]\Psi_a^{(1)} + \hat{H}^{(1)}\Psi_a^{(0)} = 0 \tag{10}$$

The second-order electronic energy of the molecule is

$$W^{BB} = \frac{e^2}{2m_e}\langle\Psi_a^{(0)}\left|\sum_{i=1}^{n}A_i{}^2\right|\Psi_a^{(0)}\rangle - \frac{e^2\hbar^2}{m_e^2}\sum_{j\neq a}(E_j^{(0)} - E_a^{(0)})^{-1} \times \left|\langle\Psi_a^{(0)}\left|\sum_{i=1}^{n}\left(\mathbf{A}\cdot\nabla + \frac{1}{2}\nabla\cdot\mathbf{A}\right)_i\right|\Psi_j^{(0)}\rangle\right|^2 = -\frac{1}{2}\xi_{\alpha\beta}B_\alpha B_\beta \tag{11}$$

where $\xi_{\alpha\beta}$ is the magnetizability tensor (eq 6).

We look for a transformation to Rebane's gauge,[41]

$$\mathbf{A} \rightarrow \mathbf{A}^{\mathscr{R}} = \mathbf{A} + \nabla f \tag{12}$$

whereby $\Psi_a^{(0)}$ is annihilated via the operator

$$0_{op} = \sum_{i=1}^{n}\left[\mathbf{A}^{\mathscr{R}}\cdot\nabla + \frac{1}{2}\nabla\cdot\mathbf{A}^{\mathscr{R}}\right]_i = \sum_{i=1}^{n}\left[\mathbf{A}\cdot\nabla + (\nabla f)\cdot\nabla + \frac{1}{2}\nabla^2 f\right]_i \tag{13}$$

assuming that $\mathbf{A}$ on the rhs of eq 13 is the vector potential in the Coulomb gauge, that is, $\nabla\cdot\mathbf{A} = 0$. Therefore, in the Rebane's gauge, the paramagnetic term of eq 11 vanishes, because

$$0_{op}\Psi_a^{(0)} = \sum_{i=1}^{n}\mathbf{A}_i\cdot\nabla_i\Psi_a^{(0)} + \sum_{i=1}^{n}(\nabla_i f)\cdot\nabla_i\Psi_a^{(0)} + \frac{1}{2}\Psi_a^{(0)}\sum_{i=1}^{n}\nabla_i{}^2 f = 0 \tag{14}$$

A solution to this equation is found observing that the invariance of the energy (eq 11) in the gauge transformation (eq 12) requires a corresponding transformation of the wave function,[60,61]

$$\Psi_a^{(0)} \rightarrow \Psi_a^{(0)}\exp\left(-\frac{ie}{\hbar}f\right) \simeq \Psi_a^{(0)} - \frac{ie}{\hbar}f\Psi_a^{(0)} \tag{15}$$

We assume that the last term on the rhs of eq 15 gives the first-order correction to the wave function via the Ansatz

$$\Psi_a^{(1)} = -\sum_{j\neq a}(E_j^{(0)} - E_a^{(0)})^{-1}\langle\Psi_j^{(0)}|\hat{H}^{(1)}|\Psi_a^{(0)}\rangle\Psi_j^{(0)} = \frac{ie}{\hbar}f\Psi_a^{(0)} \tag{16}$$

then, the condition $0_{op}\Psi_a^{(0)} = 0$, eq 14, is fulfilled allowing for eq 10 and for the zero-order equation $(\hat{H}^{(0)} - E_a^{(0)})\Psi_a^{(0)} = 0$. The generating function f has the form[5,41]

$$f = \frac{\hbar^2}{m_e}\sum_{j\neq a}(E_j^{(0)} - E_a^{(0)})^{-1}\langle\Psi_j^{(0)}\left|\sum_{i=1}^{n}(\mathbf{A}\cdot\nabla)_i\right|\Psi_a^{(0)}\rangle\frac{\Psi_j^{(0)}}{\Psi_a^{(0)}} \tag{17}$$

Therefore, within the Rebane's choice of gauge, the second-order energy (eq 11) contains only a formally diamagnetic term, the expectation value

$$W^{BB} = \frac{e^2}{2m_e}\langle\Psi_a^{(0)}|\sum_{i=1}^{n}\mathbf{A}_i^{\mathscr{R}}\cdot\mathbf{A}_i^{\mathscr{R}}|\Psi_a^{(0)}\rangle \tag{18}$$

This quadratic form is always positive, so that the trace of the magnetizability tensor $\xi_{\alpha\beta}$ is necessarily negative.

Multiplying eq 14 on the left by $f\,\Psi_a^{(0)}$ and integrating by parts, an integral "orthogonality condition" for the Rebane's gauge,

$$\langle\Psi_a^{(0)}\left|\sum_{i=1}^{n}\mathbf{A}_i^{\mathscr{R}}\cdot\nabla_i f\right|\Psi_a^{(0)}\rangle = 0 \tag{19}$$

is obtained, and allowing for relationship 19, the second-order energy can be rewritten[5]

$$\begin{aligned} W^{BB} &= \frac{e^2}{2m_e}\langle\Psi_a^{(0)}\left|\sum_{i=1}^{n}(\mathbf{A}^{\mathscr{R}}\cdot\mathbf{A})_i\right|\Psi_a^{(0)}\rangle \\ &= \frac{e^2}{2m_e}\langle\Psi_a^{(0)}\left|\sum_{i=1}^{n}(\mathbf{A}^2 - \nabla f\cdot\nabla f)_i\right|\Psi_a^{(0)}\rangle \end{aligned} \tag{20}$$

The $W^{BB} \geqslant 0$ inequality by GTB[40] rests upon the existence of the Rebane gauge function 17 and of the integrals in eqs 18−20. It is not valid if $\Psi_a^{(0)}$, appearing in the denominator of eq 17, possesses nodal surfaces, and then the Ansatz 16 is to be rejected for $n > 2$.[5]

4. CTOCD-PZ Approach

Whereas the Rebane's procedure is devised to kill the wave function $\Psi_a^{(0)}$ according to eq 14, the CTOCD-PZ procedure is based on the alternative idea that the paramagnetic contribution to the current density (eq 3) can be annihilated at any point $\mathbf{r}$ via a coordinate transformation. Since the total current density $\mathbf{J}^{\mathbf{B}} = \mathbf{J}^{\mathbf{B}}(\mathbf{r})$ is an invariant vector field, its origin can arbitrarily be chosen. Therefore, in a change of coordinate system,

$$\mathbf{r}' \rightarrow \mathbf{r}'' = \mathbf{r}' + \mathbf{d} \tag{21}$$

the diamagnetic and paramagnetic terms vary in such a way that $\mathbf{J}^{\mathbf{B}}$ remains the same,[48] that is,

$$\begin{aligned} \mathbf{J}^{\mathbf{B}}(\mathbf{r} - \mathbf{r}'') &= \mathbf{J}^{\mathbf{B}}(\mathbf{r} - \mathbf{r}') + \mathbf{J}_{\mathrm{d}}^{(\mathbf{r}''-\mathbf{r}')\times\mathbf{B}}(\mathbf{r}) + \mathbf{J}_{\mathrm{p}}^{(\mathbf{r}''-\mathbf{r}')\times\mathbf{B}}(\mathbf{r}) \\ &= \mathbf{J}^{\mathbf{B}}(\mathbf{r} - \mathbf{r}') \\ &\equiv \mathbf{J}^{\mathbf{B}}(\mathbf{r}) \end{aligned} \tag{22}$$

Consistent with eq 22, the change of the diamagnetic contribution to the current density, eq 2, is obtained by the relation[48]

$$\mathbf{J}_{\mathrm{d}}^{\mathbf{B}}(\mathbf{r} - \mathbf{r}'') = \mathbf{J}_{\mathrm{d}}^{\mathbf{B}}(\mathbf{r} - \mathbf{r}') + \mathbf{J}_{\mathrm{d}}^{(\mathbf{r}''-\mathbf{r}')\times\mathbf{B}}(\mathbf{r}) \tag{23}$$

where

$$\mathbf{J}_{\mathrm{d}}^{(\mathbf{r}''-\mathbf{r}')\times\mathbf{B}}(\mathbf{r}) = -\frac{e^2}{2m_e}(\mathbf{r}''-\mathbf{r}')\times\mathbf{B}\gamma^{(0)}(\mathbf{r}) \tag{24}$$

The corresponding transformation for the paramagnetic contribution reads

$$\mathbf{J}_{\mathrm{p}}^{\mathbf{B}}(\mathbf{r} - \mathbf{r}'') = \mathbf{J}_{\mathrm{p}}^{\mathbf{B}}(\mathbf{r} - \mathbf{r}') + \mathbf{J}_{\mathrm{p}}^{(\mathbf{r}''-\mathbf{r}')\times\mathbf{B}}(\mathbf{r}) \tag{25}$$

where

$$\begin{aligned} \mathbf{J}_{\mathrm{p}}^{(\mathbf{r}''-\mathbf{r}')\times\mathbf{B}}(\mathbf{r}) = -\frac{ne}{m_e}\int \mathrm{d}\mathbf{x}_2 \ldots \mathrm{d}\mathbf{x}_n \times \\ [(\mathbf{r}''-\mathbf{r}')\times\mathbf{B}\cdot\boldsymbol{\Psi}_a^{(\mathbf{r}''-\mathbf{r}')\times\mathbf{B}}*\hat{\mathbf{p}}\Psi_a^{(0)} + \\ \Psi_a^{(0)}*\hat{\mathbf{p}}(\mathbf{r}''-\mathbf{r}')\times\mathbf{B}\cdot\boldsymbol{\Psi}_a^{(\mathbf{r}''-\mathbf{r}')\times\mathbf{B}}] \end{aligned} \tag{26}$$

introducing the perturbed function

$$\left|\Psi_a^{(\mathbf{r}''-\mathbf{r}')\times B}\right\rangle = -\frac{e}{2m_e\hbar}\sum_{j\neq a}\omega_{ja}{}^{-1}\left|\Psi_j^{(0)}\right\rangle\langle\Psi_j^{(0)}\left|\hat{\mathbf{P}}\right|\Psi_a^{(0)}\rangle \tag{27}$$

The current density terms, eqs 24 and 26, do not depend on the origin. The constraint for invariance of the total current density is

$$\mathbf{J}_{\mathrm{p}}^{(\mathbf{r}''-\mathbf{r}')\times\mathbf{B}} + \mathbf{J}_{\mathrm{d}}^{(\mathbf{r}''-\mathbf{r}')\times\mathbf{B}} = 0 \tag{28}$$

This result holds exactly for state functions that are eigenfunctions to a model Hamiltonian, as can be proven via hypervirial relations.[48]

In eq 21 the shift of origin is represented by a constant vector $\mathbf{d}$. The CTOCD-PZ sets out to determine a general transformation function $\mathbf{d} = \mathbf{d}(\mathbf{r})$ formally annihilating the paramagnetic contribution to the current density for all $\mathbf{r}$.[44,45,62] This function can be evaluated pointwise via the condition determined from eq 25. The lhs of this equation vanishes for

$$\mathbf{J}_{\mathrm{p}}^{\mathbf{B}}(\mathbf{r} - \mathbf{r}') = -\mathbf{J}_{\mathrm{p}}^{\mathbf{d}\times\mathbf{B}}(\mathbf{r}) \tag{29}$$

which yields the 3×3 system of linear equations[44,45,62]

$$\mathbf{M}\mathbf{d} = \mathbf{T} \tag{30}$$

where

$$\begin{aligned} M_{\delta\beta} = \frac{ne}{m_e}\varepsilon_{\alpha\beta\gamma}B_\gamma\int \mathrm{d}\mathbf{x}_2 \ldots \mathrm{d}\mathbf{x}_n\,[\Psi_a^{(\mathbf{d}\times\mathbf{B})_\alpha}*\hat{p}_\delta\Psi_a^{(0)} + \\ \Psi_a^{(0)}*\hat{p}_\delta\Psi_a^{(\mathbf{d}\times\mathbf{B})_\alpha}] \end{aligned} \tag{31}$$

and

$$T_\delta = -\frac{ne}{m_e}B_\alpha\int d\mathbf{x}_2 \ldots d\mathbf{x}_n[\Psi_a^{B_\alpha}*\hat{p}_\delta\Psi_a^{(0)} + \Psi_a^{(0)}*\hat{p}_\delta\Psi_a^{B_\alpha}] \tag{32}$$

It is evident from the definition, eq 31, that the matrix $\mathbf{M}$ is singular, which means that complete annihilation of paramagnetic current is physically impossible: whereas a Larmor diamagnetic current density is always perpendicular to $\mathbf{B}$, the component of $\mathbf{J}^{\mathbf{B}}$ parallel to the magnetic field, a typically quantum mechanical quantity, does not in general vanish. However, the perpendicular component is not needed to calculate magnetic properties, eqs 6 and 7. Therefore, we only need to solve a 2×2 subsystem of eq 30 for each point in real

space to annihilate the components of the paramagnetic current on a plane perpendicular to **B**.

The analytic expression for the function $\mathbf{d} = \mathbf{d}(\mathbf{r})$ is not known in the case of approximate wave function. However, one can formally define the *n*-electron operator

$$D_\alpha = \sum_{i=1}^{n} d_{i\alpha} \tag{33}$$

having the same expectation value as the position operator $R_\alpha = \sum_{i=1}^{n} r_{i\alpha}$,

$$\langle \Psi_a^{(0)} \left| D_\alpha \right| \Psi_a^{(0)} \rangle = \langle \Psi_a^{(0)} \left| R_\alpha \right| \Psi_a^{(0)} \rangle \tag{34}$$

This identity is satisfied by optimal variational wave functions.[63]

Within the CTOCD-PZ scheme the current density contains one Larmor- and one non-Larmor-type term,

$$\mathbf{J}^{\mathbf{B}}(\mathbf{r}) = \mathbf{J}_{\mathrm{d}}^{\mathbf{B}}(\mathbf{r} - \mathbf{r}') + \mathbf{J}_{\mathrm{d}}^{\mathbf{d}\times\mathbf{B}}(\mathbf{r}) = -\frac{e^2}{2m_e}\mathbf{B} \times [\mathbf{r} - \mathbf{d}(\mathbf{r})]\gamma^{(0)}(\mathbf{r}) \tag{35}$$

Therefore, the magnetizabilities calculated via eqs 5, 6, and 35 become the sum of two addenda of the same form, the conventional Langevin-Pauli term (eq 8) and a "diamagnetic" Π contribution

$$\begin{aligned}\xi_{\alpha\delta}^{\Pi} &= \frac{1}{2}\varepsilon_{\alpha\beta\gamma}\varepsilon_{\lambda\mu\delta}\int r_\beta \mathscr{T}_{\mathrm{d}\gamma}^{(\mathbf{d}\times\mathbf{B})_\lambda}(\mathbf{r}) d_\mu(\mathbf{r})\, \mathrm{d}^3 r \\ &= \frac{e^2}{4m_e}\int \gamma^{(0)}(\mathbf{r})[d_\beta(\mathbf{r})r_\beta\delta_{\alpha\delta} - d_\alpha(\mathbf{r})r_\delta]\, \mathrm{d}^3 r \\ &= \frac{e^2}{4m_e}\langle \Psi_a^{(0)} \left| \sum_{i=1}^{n} (d_\beta r_\beta \delta_{\alpha\delta} - d_\alpha r_\delta)_i \right| \Psi_a^{(0)} \rangle \end{aligned} \tag{36}$$

which reduces to the conventional paramagnetic contribution (eq 9) of the van Vleck theory if the hypervirial momentum theorem[63] is satisfied.[44,62]

Defining the operator

$$E_{I\beta}(\mathbf{r}) = \frac{1}{4\pi\varepsilon_0} e \frac{r_\beta - R_{I\beta}}{|\mathbf{r} - \mathbf{R}_I|^3} \tag{37}$$

for the electric field exerted by an electron with position **r** on nucleus *I* at $\mathbf{R}_I$, the paramagnetic CTOCD-PZ contribution to the magnetic shielding becomes[48]

$$\begin{aligned}\sigma_{\alpha\delta}^{\Pi I} &= -\frac{1}{e}\varepsilon_{\alpha\beta\gamma}\varepsilon_{\lambda\mu\delta}\int E_{I\beta}(\mathbf{r})\mathscr{T}_{\mathrm{d}\gamma}^{(\mathbf{d}\times\mathbf{B})_\lambda}(\mathbf{r}) d_\mu(\mathbf{r})\, \mathrm{d}^3 r \\ &= -\frac{e}{2m_e c^2}\int \gamma^{(0)}(\mathbf{r})[d_\beta(\mathbf{r})E_{I\beta}(\mathbf{r})\delta_{\alpha\delta} - d_\alpha(\mathbf{r})E_{I\delta}(\mathbf{r})]\, \mathrm{d}^3 r \\ &= -\frac{e}{2m_e c^2}\langle a \left| \sum_{i=1}^{n} (d_{i\beta}E_{I\beta}^i\delta_{\alpha\delta} - d_{i\alpha}E_{I\delta}^i) \right| a \rangle \end{aligned} \tag{38}$$

This reduces to the Ramsey paramagnetic contribution[47]

$$\sigma_{\alpha\delta}^{\mathrm{p}I} = \frac{e}{2m_e c^2}\langle \Psi_a^{(0)} \left| \sum_{i=1}^{n} (r_{i\beta}E_{I\beta}^i\delta_{\alpha\delta} - r_{i\alpha}E_{I\delta}^i) \right| \Psi_a^{(0)} \rangle \tag{39}$$

for optimal variational wave functions satisfying the hypervirial theorems[44,62,63] so that

$$\sigma_{\alpha\beta}^{I} = \sigma_{\alpha\beta}^{\Pi I} + \sigma_{\alpha\beta}^{\mathrm{d}I} \tag{40}$$

The CTOCD-PZ approach does not provide any criterion to assess the relative magnitude of $\xi_{\alpha\delta}^{\mathrm{d}}$ and $\xi_{\alpha\delta}^{\Pi}$, since both cases, $r_\alpha > d_\alpha$ and $r_\alpha < d_\alpha$, are possible in eq 35. Therefore, $\xi_{\alpha\alpha}^{\Pi} \equiv \xi_{\alpha\alpha}^{\mathrm{p}}$ may be greater than $|\xi_{\alpha\alpha}^{\mathrm{d}}|$, as observed for BH and CH^+, which discounts the inequality presented by GTB.[40]

In general, the CTOCD-PZ and CTOCD-PZ2 methods do not offer any advantage of reduced computational time. However, they were found computationally efficient and superior to conventional common-origin approaches to calculate accurate nuclear magnetic shieldings via medium-size basis sets.[45]

From the invariance constraint, eq 28, and eq 29, the identity

$$\mathbf{J}_{\mathrm{d}}^{\mathbf{d}\times\mathbf{B}}(\mathbf{r}) = \mathbf{J}_{\mathrm{p}}^{\mathbf{B}}(\mathbf{r} - \mathbf{r}') \tag{41}$$

is obtained. This relationship does not provide a recipe for calculating the shift functions in the approximate case but yields the definition of exact $\mathbf{d}(\mathbf{r})$,

$$\begin{aligned} d_\gamma(\mathbf{r}) = -\frac{n}{e}[\gamma^{(0)}(\mathbf{r})]^{-1}\varepsilon_{\alpha\beta\gamma}\int \mathrm{d}\mathbf{x}_2 \ldots \mathrm{d}\mathbf{x}_n \times \\ [\Psi_a^{B_\beta *}(\mathbf{r}, \mathbf{x}_2, \ldots, \mathbf{x}_n)\hat{p}_\alpha \Psi_a^{(0)}(\mathbf{r}, \mathbf{x}_2, \ldots, \mathbf{x}_n) + \\ \Psi_a^{(0)*}(\mathbf{r}, \mathbf{x}_2, \ldots, \mathbf{x}_n)\hat{p}_\alpha \Psi_a^{B_\beta}(\mathbf{r}, \mathbf{x}_2 \ldots \mathbf{x}_n)] \end{aligned} \tag{42}$$

It is observed that the ideal killing function, eq 42, is not defined in the points of the molecular domain at which the unperturbed probability density $\gamma^{(0)}$ vanishes. Therefore paramagnetism is essential in the proximity of nodal points of the electronic wave function for a system with $n \leq 2$, and it cannot be removed via CTOCD-PZ procedures, since $[\gamma^{(0)}]^{-1}$ diverges.[44,62] On the other hand, for $n > 2$, $\gamma^{(0)}(\mathbf{r}) \neq 0$ in general. Therefore, the CTOCD-PZ approach can practically be used to annihilate the paramagnetic contribution to magnetizability and nuclear shielding in a molecule with more than two electrons; that is, it works for problems to which Rebane's approach[41,42] is inapplicable.

In addition, as shown in Section 7, for each molecular orbital in a molecule, the analysis of the nodes of the zero-order electron density can be used to detect a priori the regions where paramagnetic vortices can be expected.

5. Computational Procedures

Magnetic susceptibilities and magnetic shielding at the nuclei have been calculated at three levels of accuracy, coupled Hartree−Fock (CHF), coupled cluster singles and doubles (CCSD), and density functional theory (DFT) allowing for the Keal and Tozer KT3 functional,[64,65] implemented in the DALTON package.[66] The KT3 functional was found to be the most

TABLE 1: Calculated Magnetizabilities in ppm cgs au[a]

level	*xx*	*yy*	*zz*	*av*
		BeH^-		
CHF/CTOCD-PZ2	208.75	208.75	−423.18	−1.89
CCSD/CTOCD-DZ	155.68	155.68	−387.81	−25.48
		BH		
CHF/CTOCD-PZ2	380.64	380.64	−133.48	209.27
CCSD/CTOCD-DZ	278.45	278.45	−127.63	143.09
		CH^+		
CHF/CTOCD-PZ2	555.86	555.86	−76.46	345.09
CCSD/CTOCD-DZ	354.20	354.20	−74.16	211.41
		C_4H_4		
CHF/CTOCD-PZ2	−281.57	−240.43	−45.29	−189.10
CCSD/CTOCD-DZ	−251.76	−215.47	−53.27	−173.50
		C_8H_8		
CHF/CTOCD-PZ2	−584.96	−584.96	497.15	−224.26

[a] See the Supporting Information for CO, CTOCD-DZ, CTOCD-PZ, and CTOCD-DZ2 predictions at the CHF level and for the coordinate systems used. The conversion factor to ppm cgs per mole is $0.892\,389\,358 \times 10^{-2}$ cm^3 mol^{-1}. Further conversion to JT^{-2} mol^{-1} is obtained multiplying by 0.1. The conversion factor to SI units per molecule is $10 \times a_0^3 = 0.148\,184\,709 \times 10^{-29}$. To convert the ppm cgs au to SI au, multiply by $1.877\,886\,47 \times 10^{-2}$; further conversion to JT^{-2} per molecule is obtained multiplying by $7.891\,036\,60 \times 10^{-29}$; see ref 93.

TABLE 2: Calculated Nuclear Magnetic Shieldings, in ppm[a]

atom	level	*xx*	*yy*	*zz*	*av*
		BeH^-			
Be	CHF/CTOCD-PZ2	−51.76	−51.76	150.88	15.79
	DFT/KT3/CTOCD-DZ	−28.69	−28.69	153.26	31.96
	CCSD/CTOCD-DZ	−36.89	−36.89	150.16	25.46
H	CHF/CTOCD-PZ2	18.83	18.83	33.01	23.56
	DFT/KT3/CTOCD-DZ	19.38	19.38	32.29	23.68
	CCSD/CTOCD-DZ	19.85	19.85	32.32	24.01
		BH			
B	CHF/CTOCD-PZ2	−506.65	−506.65	198.89	−271.47
	DFT/KT3/CTOCD-DZ	−399.10	−399.10	202.30	−198.63
	CCSD/CTOCD-DZ	−379.25	−379.25	198.45	−186.69
H	CHF/CTOCD-PZ2	20.59	20.59	33.93	25.04
	DFT/KT3/CTOCD-DZ	18.22	18.22	34.15	23.53
	CCSD/CTOCD-DZ	21.42	21.42	33.52	25.45
		CH^+			
C	CHF/CTOCD-PZ2	−2030.02	−2030.02	247.08	−1270.99
	DFT/KT3/CTOCD-DZ	−1267.24	−1267.24	250.31	−761.39
	CCSD/CTOCD-DZ	−1338.52	−1338.52	246.57	−810.16
H	CHF/CTOCD-PZ2	36.34	36.34	30.97	34.55
	DFT/KT3/CTOCD-DZ	27.92	27.92	31.18	29.01
	CCSD/CTOCD-DZ	30.81	30.81	30.65	30.76
		C_4H_4			
C_1	CHF/CTOCD-PZ2	−100.68	108.96	127.23	45.17
	DFT/KT3/CTOCD-DZ	−63.39	95.90	110.89	47.80
H_1	CHF/CTOCD-PZ2	21.55	28.98	28.16	26.23
	DFT/KT3/CTOCD-DZ	22.01	27.59	28.11	25.90
		C_8H_8			
C_1	CHF/CTOCD-PZ2	−0.41	26.85	147.44	57.96
	DFT/KT3/CTOCD-DZ	2.25	31.34	112.19	48.59
H_1	CHF/CTOCD-PZ2	27.89	28.63	29.18	28.57
	DFT/KT3/CTOCD-DZ	26.48	28.02	34.15	29.55

[a] See the Supporting Information for CO, CTOCD-DZ, CTOCD-PZ, and CTOCD-DZ2 predictions at the CHF level and for the coordinate systems used.

efficient for calculating shielding constants in a series of small molecules[67] and for studies of hydrogen bonding.[68]

The common origin (CO) method and four distributed-origin CTOCD approaches have been applied. The analytic CTOCD-DZ procedure, providing origin independent nuclear shieldings, has been described elsewhere.[48] A practical variant referred to as DZ2, based on damping functions and numerical integration, is more effective and provides good displays of current density and accurate predictions of magnetic properties with medium size basis sets.[45,69] The CTOCD-DZ2 method, used to describe current density vector fields in recent applications,[70,71] has been employed to display streamline and modulus maps and stagnation graphs, Figures 1−17.

The basis sets of primitive Gaussian functions and the polarization functions employed in this study are specified in the Supporting Information. For consistency, molecular geometries were fully optimized at the HF level using the same basis sets via the GAUSSIAN package.[72] The CHF scheme implemented in the SYSMO code[73] was applied within the conventional CO, CTOCD-DZ, CTOCD-DZ2, CTOCD-PZ, and CTOCD-PZ2 procedures.[45,49] The CCSD CTOCD-DZ and DFT-KT3 CTOCD-DZ have been implemented in DALTON by Ligabue.[66]

The predictions of magnetizability of the BeH^- system were found to depend strongly on the molecular geometry, on the quality of the basis set, and on the level of approximation in previous works,[17,18] showing that both magnitude and sign of $\xi_{\alpha\beta}$ are affected. This has been confirmed in the present work for a number of extended basis sets. The results reported in Tables 1 and 2 were obtained from a high quality basis set, which provides good convergence for a number of other properties and sum rules, see the Supporting Information. The CHF predictions for the magnetizability are close to those of ref 17. The CHF components $\xi_{\parallel}$ and $\xi_{\perp}$ are sizable, but the average magnetizability nearly vanishes. CCSD CTOCD-DZ estimates for ξ_{av} were found to vary in a wide range, from ≈ 0 to ≈ -25 ppm au, depending on the basis set employed. This trend is similar to that reported in Table 4 of ref 18. Further investigations are needed to arrive at converged predictions, taking into account correlation consistent basis sets for beryllium, which lies beyond the scope of the present work.

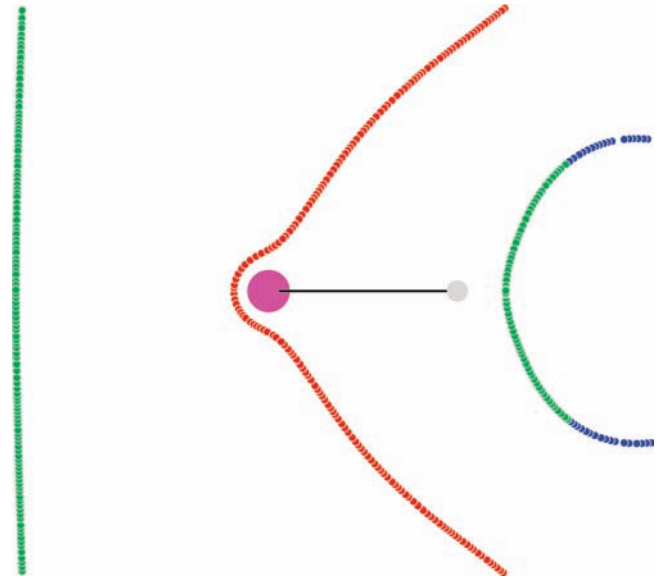

Figure 1. Stagnation graph of the BeH^- molecule in a magnetic field B_x perpendicular to the z bond axis. Here and in the following Figures 2−5, green (red) stagnation lines denote diatropic (paratropic) flow, and blue lines indicate saddle-type regime. All the stagnation lines lie on the xz plane.

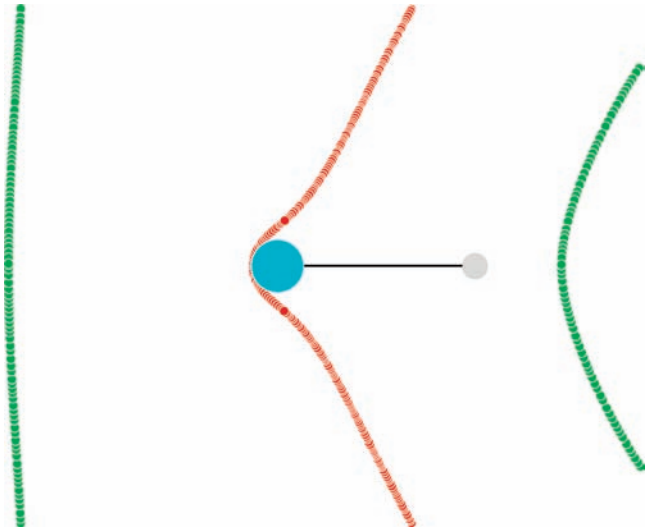

Figure 2. Stagnation graph of the BH molecule in a magnetic field B_x perpendicular to the z bond axis.

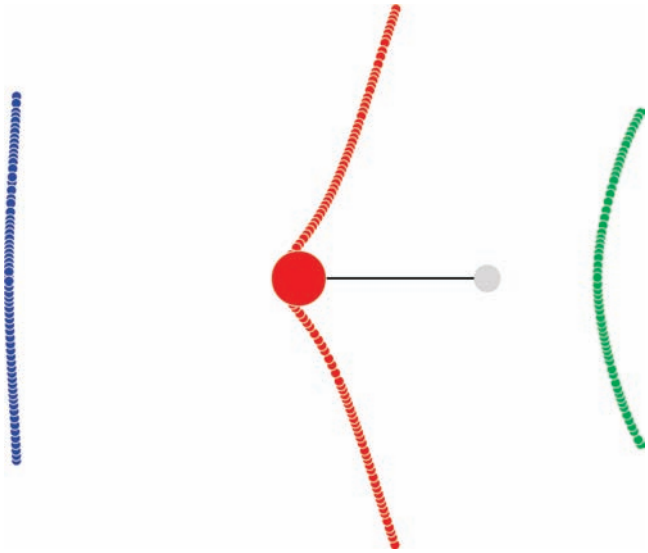

Figure 3. Stagnation graph of the CH^+ molecule in a magnetic field B_x perpendicular to the z bond axis.

On the other hand, the models developed in this study for the other compounds are of near HF quality, as proven by sum rules for gauge invariance and charge conservation and virtual identity of magnetic properties estimated by different computational schemes; see the Supporting Information. The CTOCD-PZ and CTOCD-PZ2 predictions demonstrate that also for paramagnetic systems BH and CH^+ and for π-paramagnetic planar conjugated hydrocarbons C_4H_4 and C_8H_8, the paramagnetic contribution to magnetic properties can formally be annihilated, which is not possible via the Rebane's method.[5,41]

Electron correlation is observed to bias the results to a large extent. For BeH^-, the proton shielding is almost unaffected, whereas the average shielding of the Be nucleus increases. For BH, there is a sizable decrease of ξ_{av}, CHF and CCSD CTOCD-DZ values being respectively ≈209 ppm au and ≈143 ppm au. A similar trend was also discussed by Ruud et al.[18] The KT3 and CCSD CTOCD-DZ computed values for B shielding are quite close to one another, and much smaller than CHF's; see Table 2. Analogous behavior was observed for magnetic properties of CH^+.

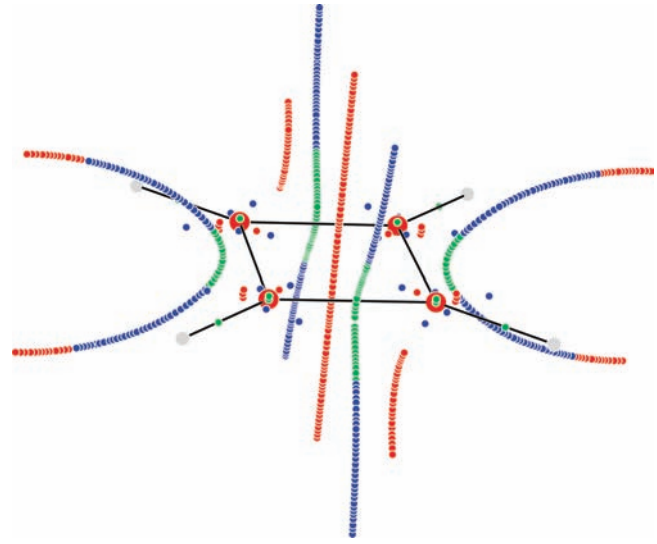

Figure 4. Perspective view of the stagnation graph of the C_4H_4 molecule in a magnetic field B_x perpendicular to the zy molecular plane.

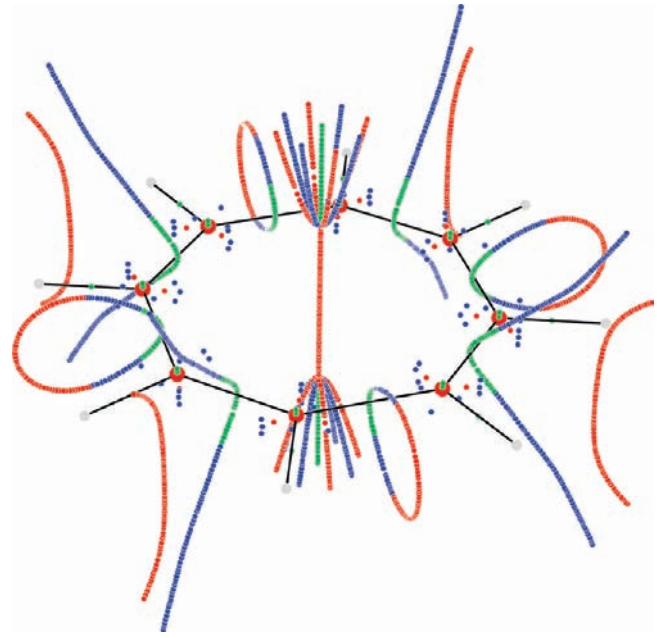

Figure 5. Perspective view of the stagnation graph of the C_8H_8 molecule in a magnetic field B_z perpendicular to the xy molecular plane. The branching points of the central stagnation line occur at $z \approx \pm 1.8$ bohr. Stagnation loops containing segments of vortex- and saddle-line are observed about the midpoint of formally single C−C bonds.

A significant decrease of $|\xi_{av}|$ and $\Delta\xi$ due to electron correlation was estimated for C_4H_4.

6. Stagnation Graphs of the Current−Density Field

The basic patterns of a $\mathbf{J}^\mathbf{B}$ field are analyzed via the phase portrait in the proximity of points at which $|\mathbf{J}^\mathbf{B}|$ vanishes. The field $\mathbf{J}^\mathbf{B}(\mathbf{r})$ in the neighborhood of a stagnation point (SP) at $\mathbf{r}_0$ is described by a truncated Taylor series,

$$J_\gamma^\mathbf{B}(\mathbf{r}) = (r_\alpha - r_{0\alpha})[\nabla_\alpha J_\gamma^\mathbf{B}]_{\mathbf{r}=\mathbf{r}_0} + \frac{1}{2}(r_\alpha - r_{0\alpha})(r_\beta - r_{0\beta})[\nabla_\alpha \nabla_\beta J_\gamma^\mathbf{B}]_{\mathbf{r}=\mathbf{r}_0} + \ldots \quad (43)$$

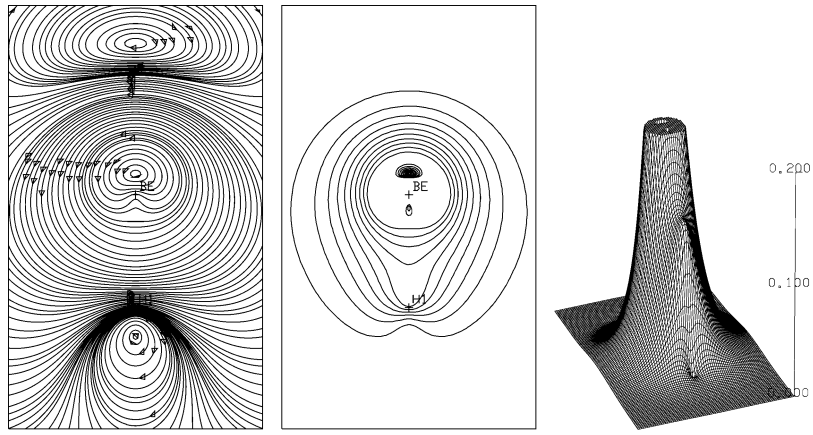

Figure 6. Current density field for BeH^- for a magnetic field B_x directed out of the yz plane containing the nuclei, with $|\mathbf{B}| = 1$ au. Diatropic (paratropic) flow is clockwise (anticlockwise). The maximum intensity $|\mathbf{J}^{\mathbf{B}}|$ is 2.20 au, truncated to 0.2 au in the contour map in the center and in the three-dimensional perspective view on the right. The step between contour levels is 0.02 au.

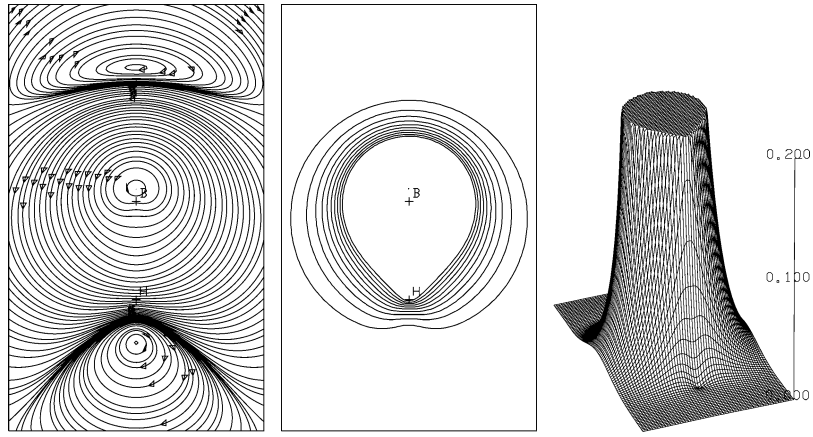

Figure 7. Current density field for BH for a magnetic field B_x directed out of the yz plane containing the nuclei, with $|\mathbf{B}| = 1$ au. The maximum intensity $|\mathbf{J}^{\mathbf{B}}|$ is 10.68 au, truncated to 0.2 au in the contour map in the center and in the three-dimensional perspective view on the right. The step between contour levels is 0.02 au. Plotting conventions are the same as in Figure 6.

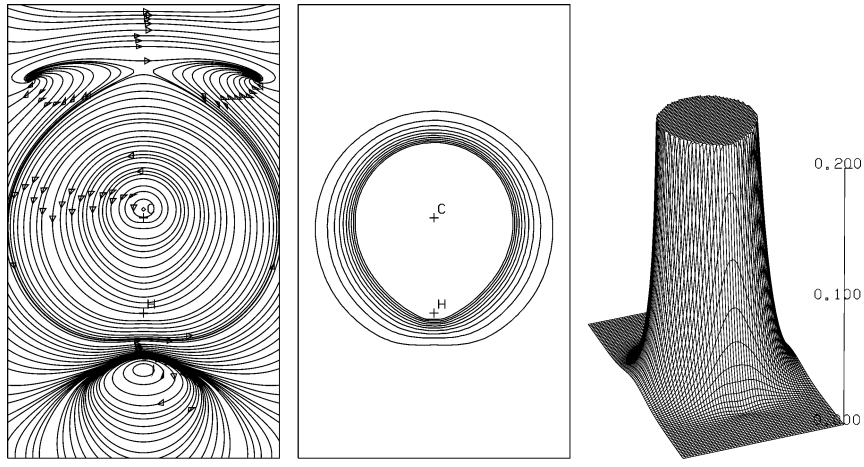

Figure 8. Current density field for CH^+ for a magnetic field B_x directed out of the yz plane containing the nuclei, with $|\mathbf{B}| = 1$ au. The maximum intensity $|\mathbf{J}^{\mathbf{B}}|$ is 33.87 au, truncated to 0.2 au in the contour map in the center and in the three-dimensional perspective view on the right. Plotting conventions are the same as in Figure 6. The step between contour levels is 0.02 au.

Reyn[74] listed all possible phase portraits in the vicinity of an SP at $\mathbf{r}_0$ in three-dimensional flow, in connection with canonical forms of the real 3×3 Jacobian matrix $\nabla_\alpha J^{\mathbf{B}}_\gamma(\mathbf{r}_0)$. The local regime depends on the eigenvalues of the Jacobian matrix. Therefore, SPs are denoted via a commonly adopted[49,75,76] (*rank*, *signature*) label,[77−79] where the rank r is defined as the number of nonvanishing eigenvalues of the Jacobian matrix and the signature s is the excess of positive over negative eigenvalues. An SP is also classified in terms of its index[80] ι.[81,82] The critical point identifications discussed here are based on the calculated eigenvalues of $\nabla_\alpha J^{\mathbf{B}}_\gamma(\mathbf{r}_0)$ for the molecules studied.

The SPs may be isolated or form continuous, open or closed, paths referred to as stagnation lines (SL). The three-dimensional structure of a current density vector field is described by the stagnation graph (SG), a topological instrument assembling all

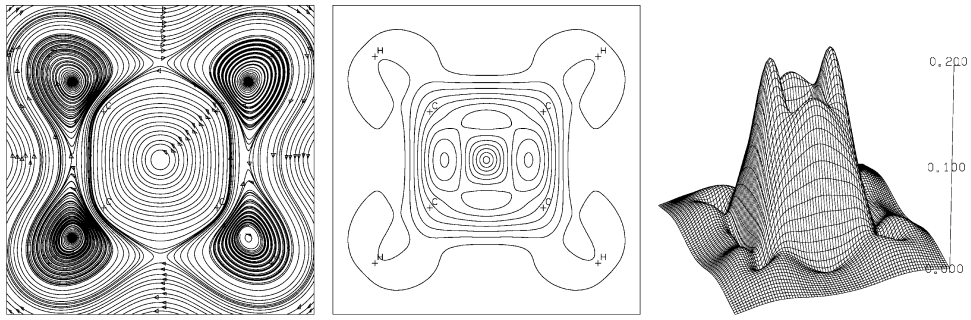

Figure 9. Current density field for C_4H_4 for a magnetic field B_x directed out of the zy molecular plane, with $|\mathbf{B}| = 1$ au. The plot plane lies 1.0 bohr above that of the nuclei, in a region of nearly maximum π-electron density. The streamline map on the left shows the central paratropic vortex, the saddle regime above the region of the C−C bonds, and the spiral flow above the C−H bonds. The maximum intensity $|\mathbf{J}^{\mathbf{B}}|$ is 0.18 au. The step between contour levels is 0.02 au. Plotting conventions are the same as in Figure 6.

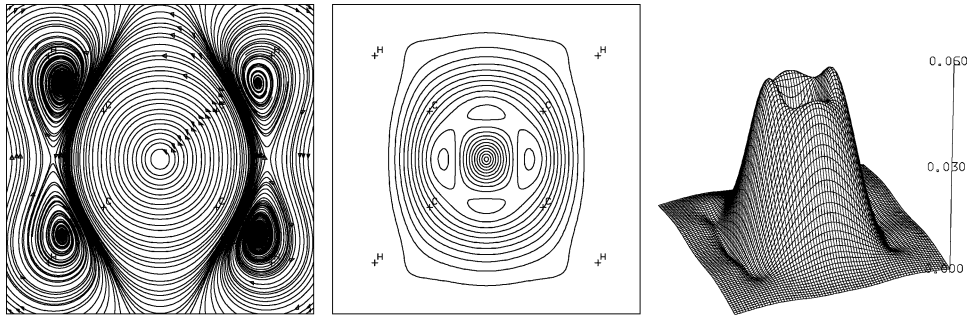

Figure 10. Current density field for C_4H_4 for a magnetic field B_x directed out of the zy molecular plane, with $|\mathbf{B}| = 1$ au. The plot plane lies 2.0 bohr above that of the nuclei. The maximum intensity $|\mathbf{J}^{\mathbf{B}}|$ is 0.05 au. The step between contour levels is 4×10^{-3} au. Plotting conventions are the same as in Figure 6.

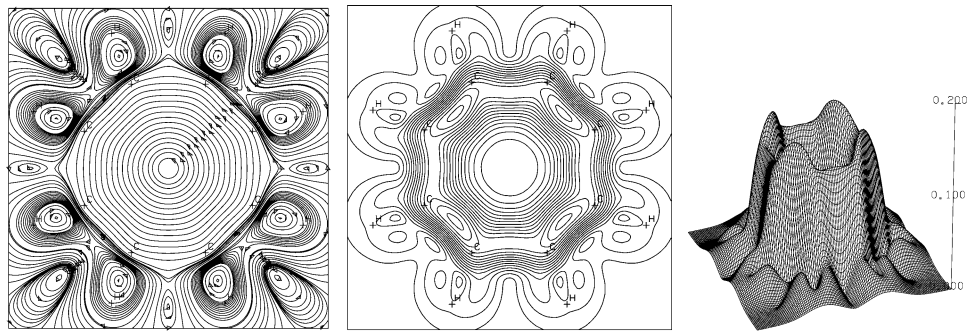

Figure 11. Current density field for flattened C_8H_8 for a magnetic field B_z directed out of the xy molecular plane, with $|\mathbf{B}| = 1$ au. The plot plane lies 1.0 bohr above that of the nuclei, in a region of nearly maximum π-electron density. The streamline map on the left shows the central paratropic vortex and the spiral flow above the C−H bonds. The maximum intensity $|\mathbf{J}^{\mathbf{B}}|$ is 0.15 au. The step between contour levels is 1×10^{-2} au. Plotting conventions are the same as in Figure 6.

isolated (3, ±1) SPs and (2, 0) SLs, which may be continuous paths of either vortex (index $\iota = +1$) or saddle (index $\iota = -1$) points.

The SGs provide fundamental information on magnetic response in relation to the $\mathbf{J}^{\mathbf{B}}$ field,[78] as shown in previous papers.[70,71,83−87] An SG illustrates branchings of an SL at (0, 0) critical points. The Gomes theorem provides an index conservation condition, $\iota_0 = \sum_{k=1}^{m} \iota_k$, for a line with index ι_0 which splits into m new lines emerging from the branching point.[78,77,79,88]

The SGs for three isoelectronic first-row hydrides in the presence of a magnetic field B_x perpendicular to the z bond axis, BeH^- in Figure 1, BH in Figure 2, and CH^+ in Figure 3, are very similar. Each contains three SLs on the zx plane, a red SL denoting a paratropic axial vortex in the vicinity of the heavier nucleus, a green SL corresponding to a diatropic vortex beyond the H nucleus, and a third SL beyond the heavier nucleus, which is vortical diamagnetic for BH and BeH^-, and saddle-type for CH^+. Direction and magnitude of the total current density induced by B_x are displayed for the yz plot plane in Figures 6−8, which show the paratropic (diatropic) vortex in the vicinity of the heavier (hydrogen) nucleus.

The SGs of C_4H_4 and COT, for a magnetic field normal to the plane of the molecule, are shown in Figures 4 and 5. Both are characterized by a central red SL, which coincides with a symmetry axis, corresponding to a paratropic axial vortex extending for several bohr in the former, and splitting into nine SLs in the latter at two points equally spaced above and below the CM at the origin. The pattern of Figure 5 for the antiaromatic COT is just the opposite of that usually observed for aromatic D_{nh} conjugated hydrocarbons, in which an external diatropic vortex splits in the vicinity of the molecular skeleton, forming vortices which end up in the regions of C−C bonds.[70]

Beyond the branching points at $z \approx \pm 1.8$ bohr one observes four red SLs in the SG of COT, corresponding to paratropic vortices, a green central line which indicates a diatropic vortex,

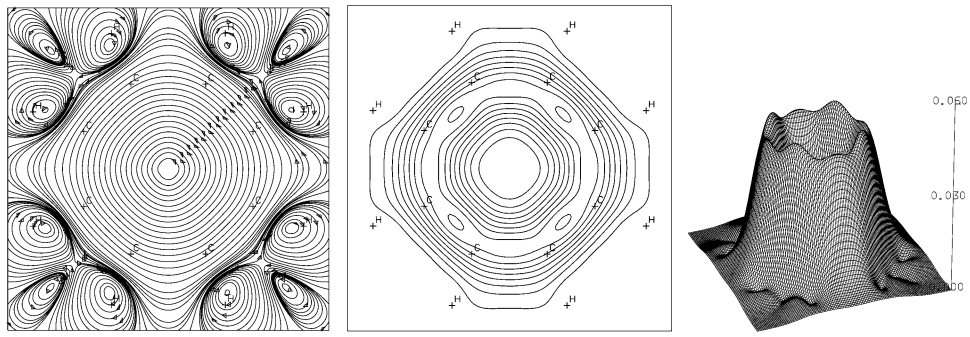

Figure 12. Current density field for flattened C_8H_8 for a magnetic field B_z directed out of the xy molecular plane, with $|\mathbf{B}| = 1$ au. The plot plane lies 2.0 bohr above that of the nuclei. The maximum intensity $|\mathbf{J}^{\mathbf{B}}|$ is 0.05 au. The step between contour levels is 5×10^{-3} au. Plotting conventions are the same as in Figure 6.

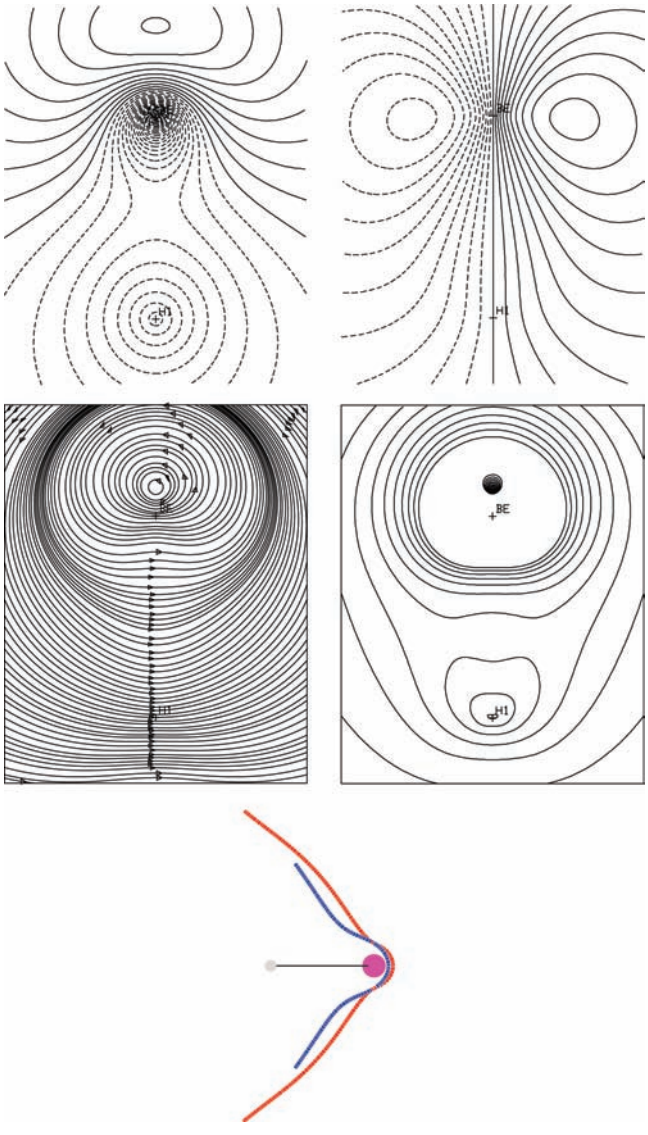

Figure 13. BeH^- anion; top-left, zero-order HOMO $\phi_3^{(0)} \equiv 3\sigma$; top-right, first-order MO $\phi_3^{(1)}$. Continuous (dashed) lines denote positive (negative) amplitude. Streamlines and magnitude of the current density $\mathbf{J}^{\mathbf{B}}$ induced in the 3σ orbital by the applied magnetic field are displayed in the center of the figure. Plotting conventions are the same as in Figure 6. Maximum intensity is 2.73 au, truncated at 0.2, and the step between two contours is 0.02. In the bottom, the blue line indicates the intersection between the nodal surfaces of $\phi_3^{(0)}$ and $\phi_3^{(1)}$, and the red line is the vortical stagnation path in Figure 1.

and four blue saddle-type SLs. The splitting process fulfills the Gomes index-conservation condition,[78] $1 = 5 - 4$.

Open SLs crossing the molecular plane and bending outward are observed about the midpoint of the C−C double bonds. They contain an internal green segment, indicating diatropic vortical flow, between two saddle SLs. The SLs about the midpoint of the C−C single bonds form closed loops, a pattern also found for the C−C bond opposite to the heteroatom in five-membered heterocyclic molecules for a magnetic field applied perpendicular to the molecular plane.[83] The SGs in in Figures 4 and 5 can be rotated and magnified for better inspection.[84]

Current density maps displaying streamlines and moduli on a few relevant planes selected with the help of the SGs in Figures 4 and 5 are displayed in Figures 9, 10, 11, and 12. These sets of figures yield nearly complete information on the structure of the magnetically induced current density field.

7. Wave Function Topology and Paramagnetism in Closed-Shell Molecules

The current density of an n electron system is characterized by the presence of vortices in $3n$-dimensional configuration space, as shown in the SGs of Figures 1−5. In three dimensions, vortices surround nodal lines at the intersection of nodal two-dimensional manifolds of real zero-order, $\phi_i^{(0)}$, and imaginary, $\phi_i^{(1)}$, first-order orbitals.[6,34]

The paramagnetism of the BH molecule has been investigated in connection with the wave function topology in refs 4, 6, and 10. According to the interpretation of Riess,[6] it is related to the intersection of the nodal surfaces of the unperturbed highest-occupied zero-order molecular orbital, $\phi_{\mathrm{HOMO}}^{(0)}$, and of the first-order $\phi_{\mathrm{HOMO}}^{(1)}$, essentially a $2p\pi$ about the B nucleus, which provide a dominant paratropic contribution. Figure 14 confirms the analysis of Riess, by showing the zero- and first-order orbitals, streamlines and modulus of the induced orbital current density, and the stagnation graph for the total $\mathbf{J}^{\mathbf{B}}$ field, which contains a red stagnation line about the B nucleus virtually coinciding with the blue line denoting the intersection of the nodal surfaces of $\phi_{\mathrm{HOMO}}^{(0)}$ and $\phi_{\mathrm{HOMO}}^{(1)}$. Inspection of Figures 13 and 15 confirms that the same interpretation in terms of nodal topology holds for BeH^- and CH^+, even if the former is less paramagnetic.

The existence of paramagnetic vortices can, in many cases, be predicted by determining orbital nodal surfaces a priori via simple symmetry arguments. In CHF theory, the ith first-order perturbed molecular orbital $\phi_i^{(1)}$ is evaluated by the corresponding unperturbed (occupied) $\phi_i^{(0)}$ via the equation[89]

$$|\phi_i^{(1)}\rangle = M^{(1)}\hat{F}^{(1)}|\phi_i^{(0)}\rangle \tag{44}$$

where

$$M^{(i)} = \sum_{k}^{VIR} (\varepsilon_i^{(0)} - \varepsilon_k^{(0)})^{-1} |\phi_k^{(0)}\rangle\langle\phi_k^{(0)}| \qquad (45)$$

is the (total symmetric) Hartree-Fock propagator, k denotes a virtual zero-order orbital, and $\hat{F}^{(1)}$ is the first-order CHF Hamiltonian.[90] Then the symmetry of $\phi_i^{(1)}$ is evaluated by the direct-product irreducible representation $\Gamma[\phi_i^{(1)}] = \Gamma[\hat{F}^{(1)}] \otimes \Gamma[\phi_i^{(0)}]$. For instance, for C_4H_4, assuming the D_{2h} symmetry and the Mulliken conventions,[91,92] the irreducible representation of the π HOMO, with orbital energy -0.2821 hartree, is $B_{2g} \approx R_y$, that of $\hat{F}^{(1)}$, for a magnetic field perpendicular to the molecular yz plane, is $B_{3g} \approx R_x$, and then the perturbed orbital has the symmetry $B_{3g} \otimes B_{2g} = B_{1g} \approx R_z$, the same as that of the lowest unoccupied molecular orbital (LUMO), with orbital energy 0.0745 hartree. Therefore, the nodal surfaces of $\phi_{\mathrm{HOMO}}^{(0)}$ and $\phi_{\mathrm{HOMO}}^{(1)}$ are, respectively, the $\sigma(xy)$ and $\sigma(zx)$ planes, intersecting along the x direction perpendicular to the molecular plane: a paramagnetic vortex is expected to flow about the nodal x axis. Figure 16 illustrating the results obtained via a Hartree-Fock calculation confirms the analysis.

Similarly, for flattened COT with D_{4h} symmetry, the representation of the π HOMO (-0.2739 hartree) is B_{1u}, that of $\hat{F}^{(1)}$, for a magnetic field perpendicular to the molecular xy plane, is $A_{2g} \approx R_z$, and then the perturbed orbital has the symmetry

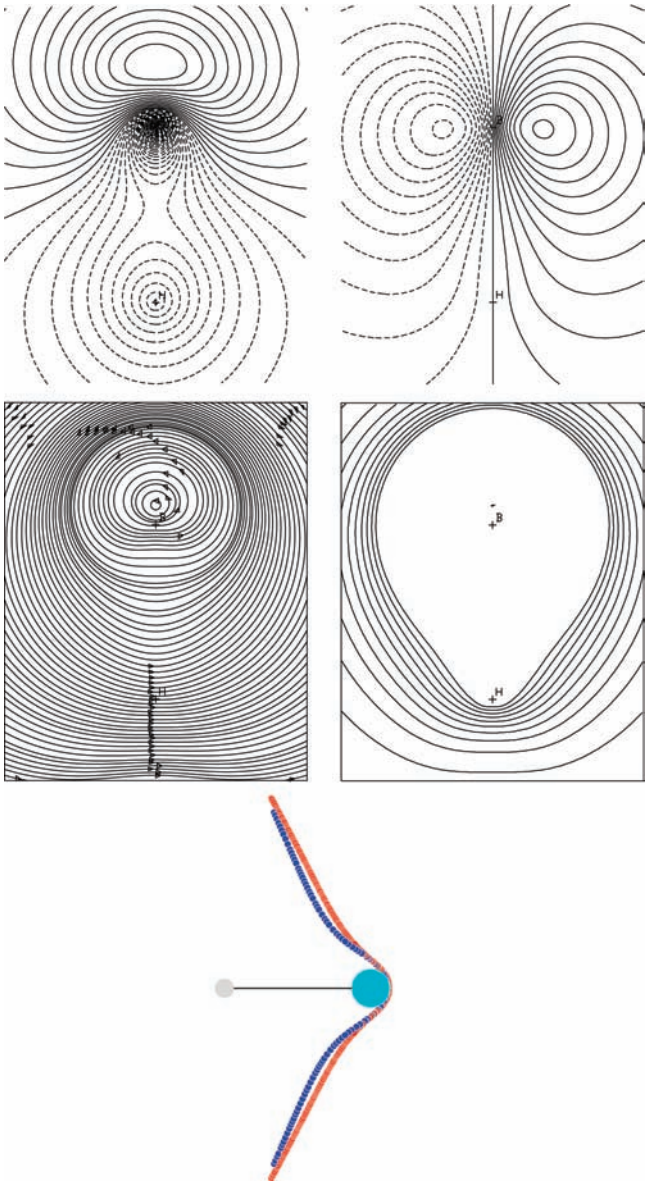

Figure 14. BH molecule; top-left, zero-order HOMO $\phi_3^{(0)} \equiv 3\sigma$; top-right, first-order MO $\phi_3^{(1)}$. Continuous (dashed) lines denote positive (negative) amplitude. Streamlines and magnitude of the current density $\mathbf{J^B}$ induced in the 3σ orbital by the applied magnetic field are displayed in the center of the figure. Plotting conventions are the same as in Figure 6. Maximum intensity is 12.08 au, truncated at 0.2, and the step between two contours is 0.02. In the bottom, the blue line indicates the intersection between the nodal surfaces of $\phi_3^{(0)}$ and $\phi_3^{(1)}$, and the red line is the vortical stagnation path in Figure 2.

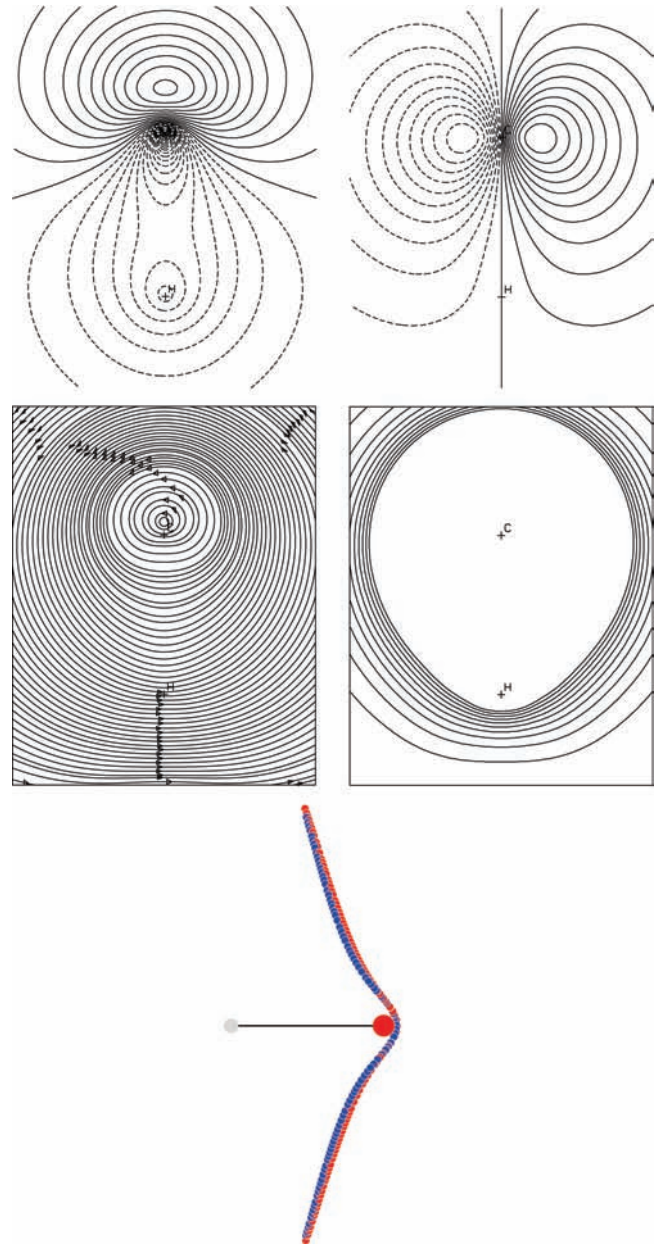

Figure 15. CH^+ cation; top-left, zero-order HOMO $\phi_3^{(0)} \equiv 3\sigma$; top-right, first-order MO $\phi_3^{(1)}$. Continuous (dashed) lines denote positive (negative) amplitude. Streamlines and magnitude of the current density $\mathbf{J^B}$ induced in the 3σ orbital by the applied magnetic field are displayed in the center of the figure. Plotting conventions are the same as in Figure 6. Maximum intensity is 35.86 au, truncated at 0.2, and the step between two contours is 0.02. In the bottom, the blue line indicates the intersection between the nodal surfaces of $\phi_3^{(0)}$ and $\phi_3^{(1)}$, and the red line is the vortical stagnation path of the total $\mathbf{J^B}$ in Figure 3.

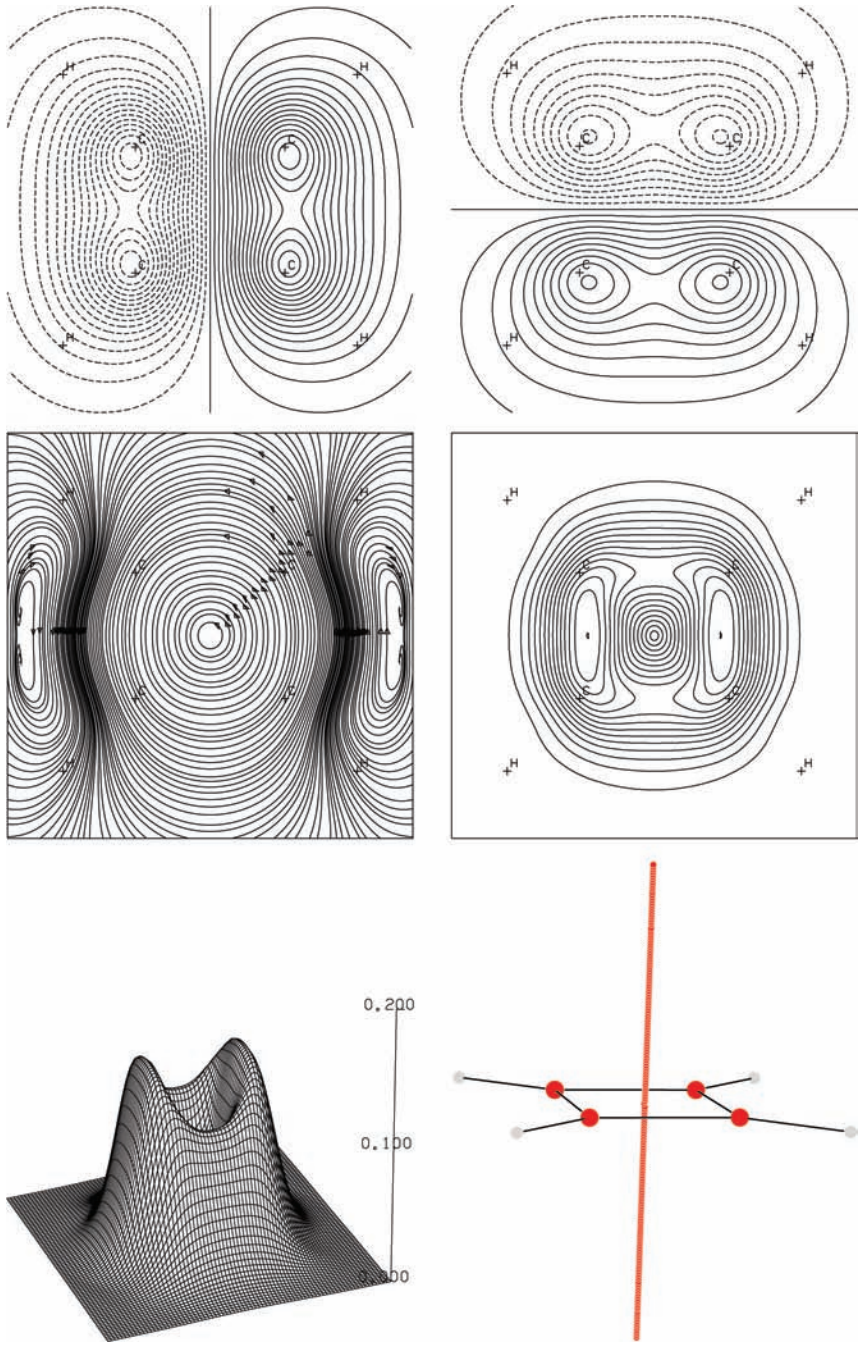

Figure 16. C_4H_4 molecule: zero-order HOMO $\phi_7^{(0)}$, with B_{2g} symmetry; top-right: first-order MO $\phi_7^{(1)}$, with B_{1g} symmetry. Continuous (dashed) lines denote positive (negative) amplitude. Streamlines and magnitude of the current density $\mathbf{J}^{\mathbf{B}}$ induced in the HOMO by the applied magnetic field on a plane 1.0 bohr above that of the molecules are displayed in the center of the figure. The corresponding three-dimensional perspective view is given in the bottom-left figure. Plotting conventions are the same as in Figure 6. Maximum intensity is 0.14 au, and the step between two contours is 0.01. In the bottom, the red line indicates the intersection between the nodal surfaces of $\phi_7^{(0)}$ and $\phi_7^{(1)}$. It coincides with the central vortical stagnation path of the total $\mathbf{J}^{\mathbf{B}}$ in Figure 4.

$A_{2g} \otimes B_{1u} = B_{2u}$, the same as the LUMO's (0.0300 hartree). The z axis perpendicular to the molecular plane lying at the intersection of several nodal planes is a vortical axis. Inspection of Figure 17 confirms the group-theoretical considerations.

8. Conclusions

A preliminary aim of this study is to show that, for any system of electrons, the approach employing a continuous transformation of the origin of the current density−paramagnetic zero[44,45,62] can be employed to formally eliminate the paramagnetic part of magnetizability and nuclear magnetic shielding considered in quantum mechanical Rayleigh−Schrödinger perturbation theory.[27,47]

Whereas the Rebane's annihilation procedure[5,41,42] can be applied only to systems with less than three electrons with nodeless state functions, the CTOCD-PZ method works for neutral molecules and molecular ions with more than two electrons, irrespective of the nodal structure of the wave function. The paramagnetic contribution to magnetic properties is efficiently killed also in paramagnetic closed-shell hydrides, for example, BH and CH^+, and in planar unsaturated hydrocarbons exhibiting π paramagnetism, for example, C_4H_4 and flattened C_8H_8. The total magnetizability of these systems can be written as a sum of two formally diamagnetic Langevin-Pauli terms, that is, as an expectation value over the unperturbed electronic wave function.

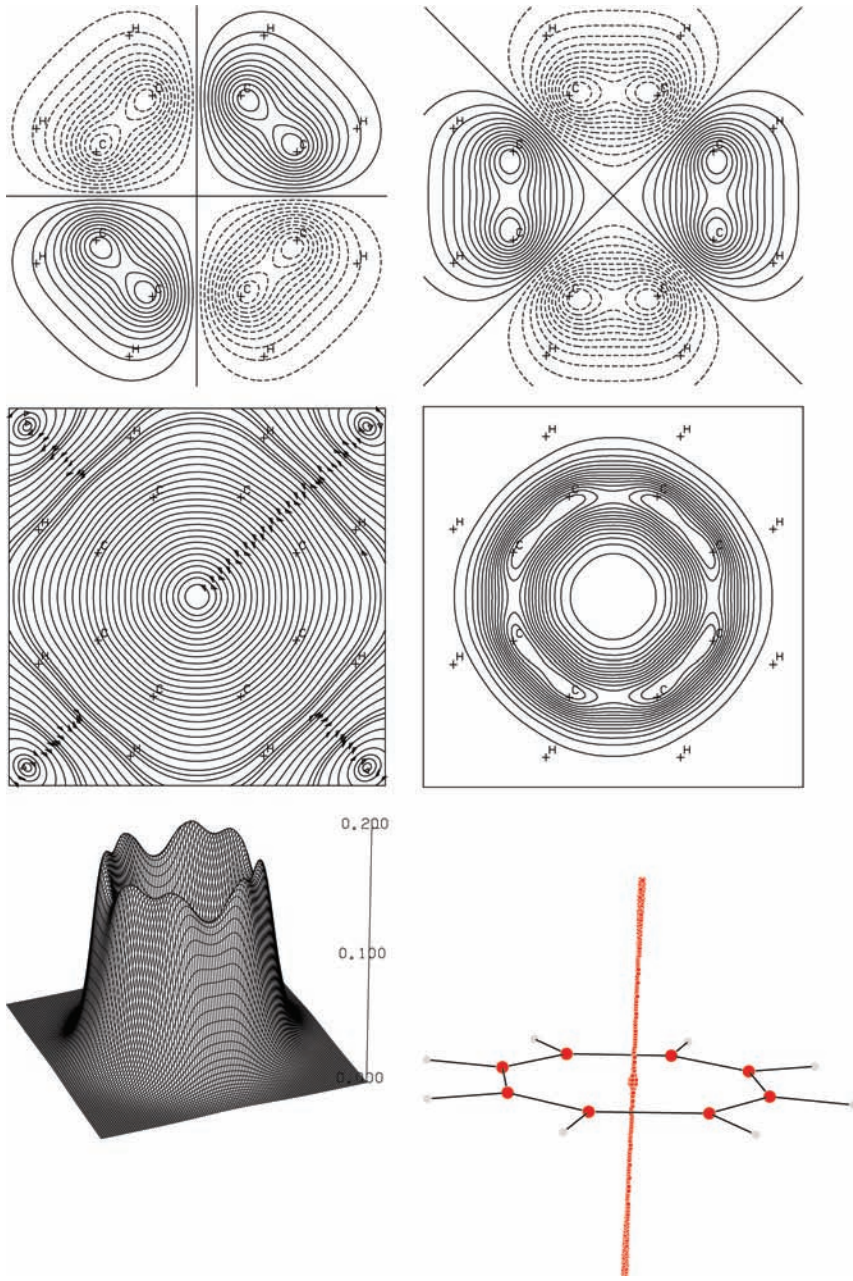

Figure 17. C_8H_8 molecule: zero-order HOMO $\phi_{16}^{(0)}$, with B_{1u} symmetry; top-right, first-order MO $\phi_{16}^{(1)}$, with B_{2u} symmetry. Continuous (dashed) lines denote positive (negative) amplitude. Streamlines and magnitude of the current density $\mathbf{J^B}$ induced in the HOMO by the applied magnetic field on a plane 1.0 bohr above that of the molecules are displayed in the center of the figure. The corresponding three-dimensional perspective view is given in the bottom-left figure. Plotting conventions are the same as in Figure 6. Maximum intensity is 0.15 au, and the step between two contours is 0.01. In the bottom, the red line indicates the intersection between the nodal surfaces of $\phi_{16}^{(0)}$ and $\phi_{16}^{(1)}$. It coincides with the central vortical stagnation path of the total $\mathbf{J^B}$ in Figure 5.

Therefore, according to Riess,[6] a system of electrons can properly be called diamagnetic (paramagnetic) if the total energy term $-(1/2)\xi_{\alpha\beta}B_\alpha B_\beta$ is positive (negative), recalling that the diamagnetic $\xi^{d}_{\alpha\beta}$ and paramagnetic $\xi^{p}_{\alpha\beta}$ contributions to the sum $\xi_{\alpha\beta} = \xi^{d}_{\alpha\beta} + \xi^{p}_{\alpha\beta}$ are not uniquely defined, as they interconvert in a gauge transformation. An analogous result was obtained for the magnetic shielding at nucleus I, $\sigma^{I}_{\alpha\beta} = \sigma^{Id}_{\alpha\beta} + \sigma^{Ip}_{\alpha\beta}$. On the other hand, the part of electronic quantum mechanical current density customarily referred to as "paramagnetic" may have any direction, providing contributions of either sign to magnetic properties from different domains of the $\mathbf{J^B}(\mathbf{r})$ field. Therefore it may more properly be called "non-Larmor", to avoid misinterpretations pointed out by Monaco and Zanasi.[39]

The second scope of the present research was to interpret the induced paramagnetism of the isoelectronic series of BeH^-, BH, and CH^+ systems, and of π-paramagnetic molecules C_4H_4 and C_8H_8. We have shown that the paramagnetic response is related to the topology of the electronic wave function. In the systems studied, paratropic vortices occur at the intersection of nodal surfaces of the zero-order HOMO with the nodal surface of the corresponding first-order perturbed orbital. The paramagnetism induced in the HOMO by a field applied at right angles to the bond axis dominates the other orbital contributions in BH and CH^+ and it bias of the total values of magnetic properties in BeH^-, C_4H_4, and C_8H_8.

Simple group-theoretical methods are sufficient to predict the occurrence of paratropic currents about the C_n symmetry axis

of a D_{nh} conjugated hydrocarbon in the presence of a magnetic field normal to the σ_h plane. Compact spatial models of the magnetic-field induced quantum mechanical current density $\mathbf{J^B}$, provided by stagnation graphs assembling isolated points and continuous sets of points at which the modulus $|\mathbf{J^B}|$ vanishes, confirm the importance of the group-theoretical analysis in systems endowed with sufficient symmetry and the practicality of the CTOCD-DZ and -PZ approaches.

Electron correlation effects estimated via KT3 DFT and CCSD approaches yield significant contributions to calculated magnetic properties. In particular, they reduce the induced paramagnetism of BH, CH^+, and C_4H_4 predicted at the CHF level. This possibly implies that also the nodal structure of the electronic wave function is affected by electron correlation, changing some features of the induced current density field and of the stagnation graph.

Acknowledgment. The authors wish to thank Dr. G. Monaco for helpful comments. Financial support to the present research from the Fondazione Cassa di Risparmio di Modena, and from the Italian MURST (Ministero dell'Università e della Ricerca Scientifica e Tecnologica), via FAR and PRIN funds, is gratefully acknowledged.

Supporting Information Available: Details of calculations, including Gaussian basis sets, molecular geometries, sum rules for gauge invariance and charge conservation, magnetizability, and nuclear magnetic shielding values. This material is available free of charge via the Internet at http://pubs.acs.org.

References and Notes

(1) Encyclopædia Britannica. http://www.britannica.com/EBchecked/topic/161370/diamagnetism.
(2) Tyndall, J. *Light and Electricity: Notes of Two Courses of Lectures Before the Royal Institution of Great Britain*; University of Wisconsin: Madison, WI, 1895; Digitized Jan 3, 2008, by D. Appleton and Co., http://books.google.com/books.
(3) Stevens, R. M.; Lipscomb, W. N. *J. Chem. Phys.* **1965**, *42*, 3666–3669.
(4) Hegstrom, R. A.; Lipscomb, W. N. *J. Chem. Phys.* **1966**, *45*, 2378–2383.
(5) Hegstrom, R. A.; Lipscomb, W. N. *Rev. Mod. Phys.* **1968**, *40*, 354–358.
(6) Riess, J. *Ann. Phys.* **1970**, *57*, 301–321.
(7) Riess, J. *Ann. Phys.* **1971**, *67*, 346–347.
(8) Lipscomb, W. N. *MTP Int. Rev. Sci. Phys. Chem.* **1972**, *1*, 167.
(9) Žaucer, M.; Pumpernik, D.; Hladnik, M.; Ažman, A. *Chem. Phys. Lett.* **1977**, *48*, 139–140.
(10) Heller, D. F.; Hirschfelder, J. O. *J. Chem. Phys.* **1977**, *66*, 1929–1933.
(11) Jaszuński, M. *Theor. Chim. Acta* **1978**, *48*, 323–329.
(12) Corcoran, C. T.; Hirschfelder, J. O. *J. Chem. Phys.* **1980**, *72*, 1524–1528.
(13) Schindler, M.; Kutzelnigg, W. *J. Chem. Phys.* **1982**, *76*, 1919–1933.
(14) Daborn, G. T.; Handy, N. C. *Mol. Phys.* **1983**, *49*, 1277–1288.
(15) Fowler, P. W.; Steiner, E. *Mol. Phys.* **1991**, *74*, 1147–1158.
(16) Sauer, S. P. A.; Oddershede, J.; Geertsen, J. *Mol. Phys.* **1992**, *76*, 445–465.
(17) Sauer, S. P. A.; Enevoldsen, T.; Oddershede, J. *J. Chem. Phys.* **1993**, *98*, 9748–9757.
(18) Ruud, K.; Helgaker, T.; Bak, K. L.; Jørgensen, P.; Olsen, J. *Chem. Phys.* **1995**, *195*, 157–169.
(19) Bally, T.; Masamune, S. *Tetrahedron* **1980**, *36*, 343–370.
(20) Pelloni, S.; Ligabue, A.; Lazzeretti, P. *Org. Lett.* **2004**, *6*, 4451–4454.
(21) Einstein, F. W. B.; Willis, A. C.; Cullen, W. R.; Soulen, R. L. *J. Chem. Soc., Chem. Comm.* **1981**, 526–528.
(22) Matsuura, A.; Komatsu, K. *J. Am. Chem. Soc.* **2001**, *123*, 1768–1769.
(23) Nishinaga, T.; Uto, T.; Matsuura, R. I. A.; Treitel, N.; Rabinovitz, M.; Komatsu, K. *Chem.—Eur. J.* **2001**, *14*, 2067–2074.
(24) Jartín, R. S.; Ligabue, A.; Soncini, A.; Lazzeretti, P. *J. Phys. Chem. A* **2002**, *106*, 11806–11814.
(25) Cuesta, I. G.; Ligabue, A.; Sánchez de Merás, A.; Lazzeretti, P. *Chem. Phys. Lett.* **2005**, *401*, 282–287.
(26) Monaco, G.; Scott, L. T.; Zanasi, R. *J. Phys. Chem. A* **2008**, *112*, 8136–8147.
(27) van Vleck, J. H. *The Theory of Electric and Magnetic Susceptibilities*; Oxford University Press: Oxford, 1932.
(28) A number of authors, including W. Voigt, J. J. Thomson, and R. Gans, are mentioned in ref 27. Van Vleck noted that many of the van Leeuwen's results had been previously discussed by N. Bohr in his dissertation.
(29) Feynman, R. P.; Leighton, R. B.; Sands, M. *The Feynmam lectures on physics*; Addison-Wesley: Reading, MA, 1966; Vol. II, p 34-2.
(30) Hirschfelder, J. O.; Christoph, A. C. *J. Chem. Phys.* **1974**, *61*, 5435–5455.
(31) Hirschfelder, J. O.; Goebel, C. J.; Bruch, L. W. *J. Chem. Phys.* **1974**, *61*, 5456–5459.
(32) Hirschfelder, J. O.; Tang, K. T. *J. Chem. Phys.* **1976**, *64*, 760–785.
(33) Hirschfelder, J. O.; Tang, K. T. *J. Chem. Phys.* **1976**, *65*, 470–486.
(34) Hirschfelder, J. O. *J. Chem. Phys.* **1977**, *67*, 5477–5483.
(35) Riess, J. *Phys. Rev. B* **1976**, *13*, 3862–3869.
(36) Riess, J.; Primas, H. *Chem. Phys. Lett.* **1968**, *1*, 545–548.
(37) That is, the molecule does not possess a permanent orbital contribution to the magnetic moment.
(38) Flygare, W. H. *Chem. Rev.* **1974**, *74*, 653–687.
(39) Monaco, G.; Zanasi, R. *Int. J. Quantum Chem.* **2009**, *109*, 243–249.
(40) Guy, J.; Tillieu, J.; Baudet, J. *C. R. Acad. Sci. (Paris)* **1958**, *246*, 574–576.
(41) Rebane, T. K. *Soviet Phys. JETP* **1960**, *11*, 694–695. [*Zh. Eksperim. i Teor. Fiz.* **1960**, *38*, 963, Engl. translation].
(42) Hameka, H. F. *Advanced Quantum Chemistry*; Addison-Wesley: Reading, MA, 1965; pp 157−167.
(43) Zanasi, R.; Lazzeretti, P.; Malagoli, M.; Piccinini, F. *J. Chem. Phys.* **1995**, *102*, 7150–7157.
(44) Lazzeretti, P.; Zanasi, R. *Int. J. Quantum Chem.* **1996**, *60*, 249–259.
(45) Zanasi, R. *J. Chem. Phys.* **1996**, *105*, 1460–1469.
(46) Landau, L. D.; Lifshitz, E. M. *Quantum Mechanics*; Pergamon Press: Oxford, 1981.
(47) Ramsey, N. F. *Phys. Rev.* **1950**, *78*, 699–703.
(48) Lazzeretti, P.; Malagoli, M.; Zanasi, R. *Chem. Phys. Lett.* **1994**, *220*, 299–304.
(49) Lazzeretti, P. Ring Currents. In *Progress Nuclear Magnetic Resonance Spectroscopy*; Emsley, J. W., Feeney, J., Sutcliffe, L. H., Eds.; Elsevier: New York, 2000; Vol. 36.
(50) Tillieu, J.; Guy, J. *C. R. Acad. Sci. (Paris)* **1954**, *239*, 1203–1205.
(51) Guy, J.; Tillieu, J. *J. Chem. Phys.* **1956**, *24*, 1117–1117.
(52) Tillieu, J. *Ann. Phys. (Paris)* **1957**, *2*, 471–497.
(53) Tillieu, J. *Ann. Phys. (Paris)* **1957**, *2*, 631–675.
(54) Karplus, M.; Kolker, H. J. *J. Chem. Phys.* **1961**, *35*, 2235–2236.
(55) Das, T. P.; Karplus, M. *J. Chem. Phys.* **1962**, *36*, 2275–2281.
(56) Hurst, R. P.; Karplus, M.; Das, T. P. *J. Chem. Phys.* **1962**, *36*, 2786–2792.
(57) Chan, S. I.; Das, T. P. *J. Chem. Phys.* **1962**, *37*, 1527–1533.
(58) Karplus, M.; Kolker, H. J. *J. Chem. Phys.* **1963**, *38*, 1263–1275.
(59) Kolker, H. J.; Karplus, M. *J. Chem. Phys.* **1964**, *41*, 1259–1266.
(60) Fock, V. *Z. Phys.* **1926**, *39*, 226–232.
(61) Jackson, J. D.; Okun, L. B. *Rev. Mod. Phys.* **2001**, *73*, 663–680.
(62) Lazzeretti, P. Electric and Magnetic Properties of Molecules. In *Handbook of Molecular Physics and Quantum Chemistry*; John Wiley & Sons, Ltd.: Chichester, 2003; Vol. 3, Part 1, Chapter 3.
(63) Epstein, S. T. *The Variation Method in Quantum Chemistry*; Academic Press: New York, 1974.
(64) Keal, W.; Tozer, D. J. *J. Chem. Phys.* **2003**, *119*, 3015–3024.
(65) Keal, W.; Tozer, D. J. *J. Chem. Phys.* **2004**, *121*, 5654–5660.
(66) DALTON, An electronic structure program, Release 2.0; 2005 (http://www.kjemi.uio.no/software/dalton/).
(67) Ligabue, A.; Sauer, S. P. A.; Lazzeretti, P. *J. Chem. Phys.* **2007**, *126*, 154111–154114.
(68) Kongsted, J.; Aidas, K.; Mikkelsen, K. V.; Sauer, S. P. A. *J. Chem. Theor. Comp.* **2008**, *4*, 267–277.
(69) Keith, T. A.; Bader, R. F. W. *Chem. Phys. Lett.* **1993**, *210*, 223–231.
(70) Pelloni, S.; Faglioni, F.; Zanasi, R.; Lazzeretti, P. *Phys. Rev. A* **2006**, *74*, 012506.
(71) Pelloni, S.; Lazzeretti, P. *J. Chem. Phys.* **2008**, *128*, 194305-1–194305-10.
(72) Frisch, M. J.; Trucks, G. W.; et al. *Gaussian 2003*, Revision B.05; Gaussian, Inc.: Pittsburgh, PA, 2003.
(73) Lazzeretti, P.; Malagoli, M.; Zanasi, R. Technical Report on Project "Sistemi Informatici e Calcolo Parallelo", Research Report 1/67, CNR, 1991.

(74) Reyn, J. W. *Z. Angew. Math. Physik* **1964**, *15*, 540–557.
(75) Keith, T. A.; Bader, R. F. W. *J. Chem. Phys.* **1993**, *99*, 3669–3682.
(76) Bader, R. F. W.; Keith, T. A. *J. Chem. Phys.* **1993**, *99*, 3683–3693.
(77) Gomes, J. A. N. F. *J. Chem. Phys.* **1983**, *78*, 4585–4591.
(78) Gomes, J. A. N. F. *Phys. Rev. A* **1983**, *28*, 559–566.
(79) Gomes, J. A. N. F. *J. Mol. Struct. (THEOCHEM)* **1983**, *93*, 111–127.
(80) The topological index ι counts the number of times that the current density vector $\mathbf{J^B}$ rotates completely while one walks counterclockwise around a circle of radius ε, so small that $\mathbf{J^B}$ has no zeroes inside except the SP at its center. The topological index ι of a saddle (vortex) line is -1 ($+1$). Both SPs have $(r,s) = (2,0)$.
(81) Milnor, J. W. *Topology from the Differentiable Viewpoint*; University of Virginia Press: Charlottesville, VA, 1997.
(82) Guillemin, V.; Pollack, A. *Differential Topology*; Prentice Hall: Englewood Cliffs, 1974.
(83) Pelloni, S.; Lazzeretti, P. *Theor. Chem. Acc.* **2007**, *117*, 903–913.
(84) The LINUX and WINDOWS versions of the graphic code used to obtain three-dimensional representations of the SG can be downloaded at https://theochem.chimfar.unimo.it/VEDO3/JPCA.jp903859k.
(85) Pelloni, S.; Lazzeretti, P.; Zanasi, R. *J. Phys. Chem. A* **2007**, *111*, 8163–8169.
(86) Pelloni, S.; Lazzeretti, P. *J. Phys. Chem. A* **2008**, *112*, 5175–5186.
(87) Pelloni, S.; Lazzeretti, P. *Chem. Phys.* **2009**, *356*, 153–163.
(88) Gomes, J. A. N. F.; Mallion, R. B. *Chem. Rev.* **2001**, *101*, 1349–1383.
(89) LazzerettI, P. *Int. J. Quantum Chem.* **1978**, *13*, 375–390.
(90) Lazzeretti, P.; Malagoli, M.; Zanasi, R. *J. Mol. Struct. (Theochem)* **1991**, *234*, 127–145.
(91) *J. Chem. Phys.* **1955**, *23*, 1997−2011.
(92) Mulliken, R. S. *J. Chem. Phys.* **1956**, *24*, 1118–1118.
(93) Mohr, P. J.; Taylor, B. N. *Rev. Mod. Phys.* **2005**, *77*, 1–107.

JP903859K